Chapter 5

5 Seismic Hazard in Mérida

5.1 Introduction

In this chapter, the assessment procedure for seismic hazard is performed, first, identifying the sources of seismic activity and their recurrence and power, based on a probabilistic analysis of maximum values in seismic catalogs, the scenario events are selected through this approach, and are used to estimate the surface response of the soils in Mérida's plateau, by means of an Equivalent Linear site-response analysis software. Potential local effects such as liquefaction and landsliding are also assessed for Mérida's tableau through a specific methodology: HAZUS®99 Earthquake Loss Estimation Methodology.

5.2 Tectonic Environment and Seismicity in Venezuela

Northern Venezuela is considered part of the boundaries between the South American and Caribbean plates. Over the continental platform this boundary is characterized by a faulting system oriented approximately E-W through the coast and Coastal Mountain range and SW-NE through the Andean Mountain range. The Andean Mountain Chains are identified as a subduction zone of the Caribbean under the South American plate characterized by being a multi-branched plate boundary located in Southwestern Caribbean and Northwestern Venezuela called the Boconó Fault Zone (identified as **B** in Figure 5.). The main trace of the Boconó Fault Zone (BFZ) as well as the sub parallel secondary faults, are NE oriented right-lateral strike-slip faults (RLSS). The Coastal Mountain Chains are composed by a series of E-W striking, right-lateral strike-slip (RLSS) faults including the Oca fault zone (northeast), the San Sebastián-La Victoria fault zone (north central Venezuela) and the El Pilar fault (easterly) [Pérez et al., 1997], each of them identified as **O**, **LV** and **EP** respectively, in Figure 5.1.

This tectonic stripe of about 100 km wide and 1,500 km long is identified as the Boconó-Oca-Morón-El Pilar Fault System, constituted by the four Fault Zones indicated by its name. The most important tectonic-topographic features participating in plate limits are: the Santa Marta Mountain Chain (Colombia), the eastern Colombian mountain range, the Perijá Sierra, the Maracaibo lake Basin, the Venezuelan Andes, the Falcón Basin, and the Caribbean Mountains. Relative displacement of South America towards west with respect the Caribbean generates compression stress on the earth crust in an E-W direction. In faults composing the Fault System in Venezuela, displacement velocity depends on particular orientation of the

fault zones with respect to the principal direction of stress (E-W). The most populated zone of Venezuela with several principal cities is located in this tectonic arch over the mountain ranges. Seismicity in this tectonic stripe evidences the presence of active faults in its longitude, configuring seismogenic zones with different power and recurrence of energy liberation. Evidence of active faulting not only lies on seismic activity, but also in geologic records and specific topographic and geomorphologic features [Kramer, 1996], being in this case characteristic features in the principal trace of the fault system. Due to the facts described above this seismic-tectonic axis constitutes an important zone of seismic hazard in Venezuela, affecting urban and rural areas.

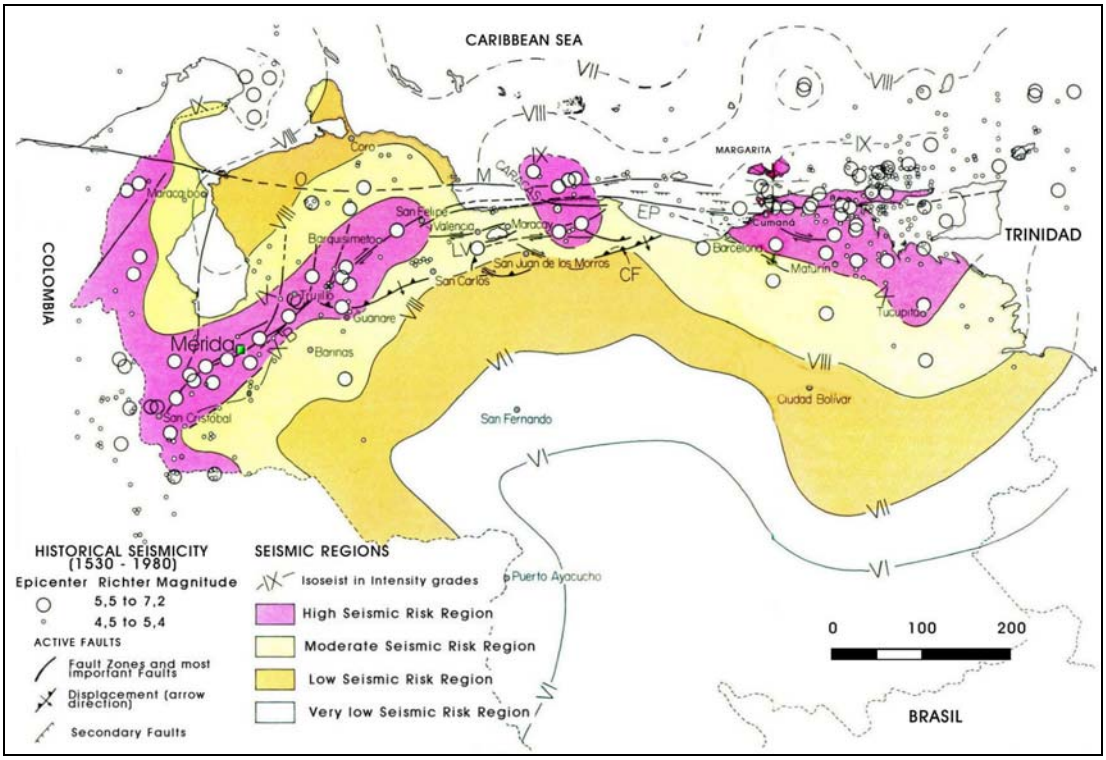

Figure 5.1: Historical Seismicity Map for Venezuela (after [Schubert, 1984]).

Historical events registered for Venezuela between 1530 and 1997 collect a series of damaging earthquakes. Along this period, about 130 events have generated damage to some extent, being Caracas, Cumaná and Mérida the most affected cities. Considerable human losses and destruction has been reported [Rendón et. al., 1997]. The most destructive earthquakes for Venezuela in this period are presented in Table 5.1. Descriptors identify the date, the most affected locations, the MMI intensity, the inferred Richter magnitude, and any relevant earthquake effects. It is important to notice that eight out of the twenty earthquakes (~ 40%) have occurred in the northeastern region of Venezuela.

In the 20th century, two important damaging earthquakes have occurred in Venezuela, triggering for each case, special measures from the government after evaluating the damage generated by the inadequate seismic performance of buildings and the occurrence of local site effects. Those earthquakes are:

- The Caracas July 29, 1967 earthquake, with a *Ms* = 6.5 magnitude, occurred in the Caribbean Sea northerly of Venezuela with epicenter coordinates 67.25W-11.0N and focal depth estimated to be 30.0 kilometers. The earthquake occurred at 20:05 hrs (local time) and the duration was 35 sec. The most affected zones were the Caracas

Metropolitan area (MMI Intensity VI-VII) and also cities and towns in the Central Coastal Line (MMI Intensities VIII or more). With 245 dead and 2,000 injured, total damage cost rounded $50 million (U.S. currency). Housing buildings from old houses to modern buildings with heights greater than two stories were reported damaged. The total number of buildings damaged was 2,635. No other civil constructions, such as elevated water tanks, bridges, etc. were damaged [FUNVISIS, 1978].

- The Caríaco July 09, 1997 earthquake, a strong event with a *Ms* = 6.8 magnitude, epicenter coordinates 63.515W-10.545N and depth estimated as 9.4 km. Time and duration were 15:24 hrs and 40 sec, respectively. Maximum intensity for epicentral area between Caríaco and Cumaná has been estimated as ***I*** (EMS) = VIII. Earthquake generated 74 casualties; most of them in 2 schools in Caríaco and a seven-story residential building in Cumaná, the number of injured was 522 people and more than 2,000 people were homeless. Partial or total collapse as well as considerable damage to structures occurred, particularly in the cities mentioned above. Severe damage to water, electricity and road lifelines occurred due to fault rupture (coseismic displacement of 0.25 m) and liquefaction (in the coastal line). Total damaged buildings rose up to 6,400 distributed most of them in dwellings (approximately 6,000) and educational facilities (381); destruction of houses was concentrated in bahareque building type (earthen wall structure), 50% of total buildings should be substituted, in educational facilities, 29 were substituted and the rest repaired or partially reconstructed. Damage to health facilities was negligible to slight [FUNVISIS, 1997; Rangel, 1999; Bonilla et. al. 2000; Castilla and Marinilli, 2000].

Seismicity monitoring in Venezuela is quite recent, the Caracas July 29, 1967 earthquake is a reference for seismological research. Prior to the earthquake, eight seismological stations (conventional type) existed, managed by national observatories. The consequences of the earthquake woke a national interest and made clear the need for further seismological research; the Venezuelan Foundation of Seismological Research (FUNVISIS) was created by a National government decree to study and monitor seismic activity in the country, with the responsibility to manage the National Seismological Network (RESVAC: Red Sismológica Venezolana con Apertura Continental). The project for national seismological array began activities in 1981, incorporating all existing stations with ten telemetric stations for short periods located through the North-Central region of the country. Parallel to these, local networks were also created by other institutions (Universities, Electric Power Companies and Oil Companies) to complement seismic monitoring and data acquisition. Data from this national array, as well as local arrays monitoring since 1982, the world network prior to 1982, and historical events chronicles, comprise the Venezuelan Seismic Catalog.

A map for the National Seismological Array is shown in Figure 5.2, with the corresponding managing institutions. These are: FUNVISIS (black triangles): National Foundation of Seismological Research; PDVSA-RESCOLM (blue triangles): Petróleos de Venezuela S.A. (national oil company) and Eastern Coast of Maracaibo lake networks; DESURCA (red triangles): Uribante-Caparo hydroelectric complex network; ULA (violet triangles): University of The Andes network; GURI (green triangles): Guri River hydroelectric complex network; and UDO (brown triangles): Eastern University network. An updated isoseismal intensity map for Venezuela is not available at the moment; although in (Schubert, 1983) a map previous to the 1997 Caríaco earthquake shows how historical events are distributed in Venezuelan geography (Figure 5.1). Isoseismal curves (for intensity) and traces for the principal fault systems are depicted. It is evident that seismic activity has been important from colonial times, configuring high to moderate seismic risk regions that support the idea of the tectonic stripe described previously.

Date (yy-mm-dd)	Most affected Location	MMI Intensity	Magnitude	Effects
1530-09-01	Cumaná	X	-	Tsunami, many people dead
1610-02-03	La Grita	IX	-	60 people dead
1641-06-11	Cúa, Miranda State	IX	6.3	Town had to be moved, 200 people dead
1684-05-04	Cumaná	VIII	-	Building damage
1766-10-21	Carúpano	VIII	7.9	Damage and casualties
1794-09-10	Cumaná	VIII	6.0	Four fifths of the city was destroyed
	Mérida	IX	7.2	5,000 casualties
1812-03-26	San Felipe	X	7.2	4,000 casualties, River Yurubí dammed
	Caracas & La Guaira	VIII to IX	6.8	10,000 casualties
1849-02-26	Lobatera	IX	6.0	40 to 50 people dead
1853-07-15	Cumaná	IX	6.7	Tsunami, 113 people dead
1870-06-26	El Tocuyo	VIII	6.1	3 casualties
1874-08-17	El Pilar, Sucre State	VIII	6.1	Damage in buildings, total damage in Church
1875-05-18	San Cristóbal	VIII	7.3	2,500 casualties, most of them in Cúcuta, Colombia
1878-04-14	Cúa	IX	6.2	400 casualties
1894-04-28	Santa Cruz	IX	7.0	319 casualties
1900-10-29	Carenero	IX	7.6	40 people dead
1929-01-17	Cumaná	IX	6.9	Tsunami, damage in the city, 50 people dead and 800 injured
1950-08-03	El Tocuyo	IX	6.8	15 casualties
1967-07-29	Caraballeda & Caracas	VIII	6.3	285 people dead, collapsed buildings; estimated loss: US$ 100 Million
1989-04-30	Boca del Tocuyo, Falcón State	VII	5.9	Important damage in churches schools and houses. Liquefaction was observed
1997-07-09	Caríaco & Cumaná	VIII	6.8	74 people dead, five collapsed buildings and more than 200 houses suffered damage. Estimated losses: US$ 100 Million

Table 5.1: Relevant destructive earthquakes in Venezuela, from 1530 to 1997.

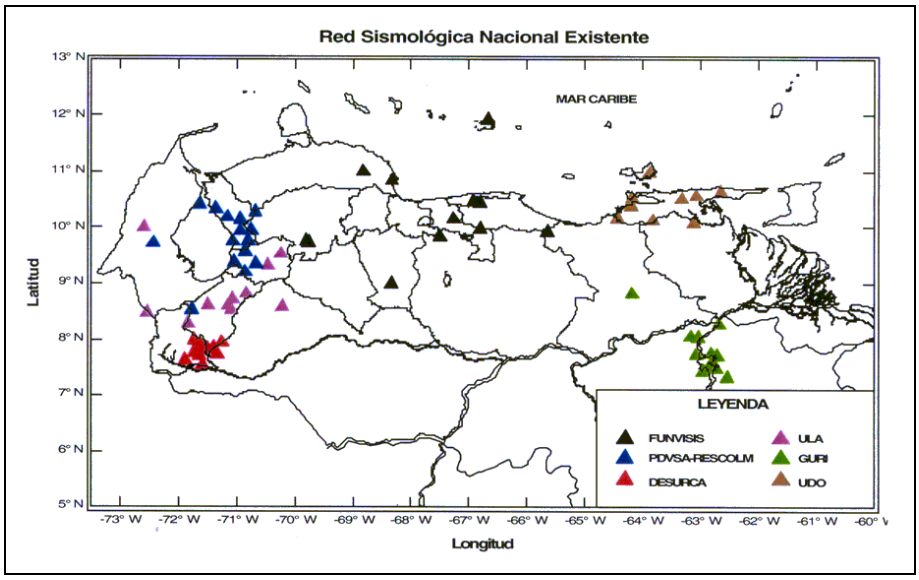

Figure 5.2: National Seismological Array for Venezuela (downloaded from: http://www.funvisis.org.ve/red_sismologica_nacional.html).

Considering the differences between the seismic zonation maps for Venezuela included in the present seismic code: Norma Covenin 1756-98 [MINDUR and FUNVISIS, 1998], and those in the previous code: Norma Covenin-Mindur-Funvisis, 1756-82 [MINDUR and FUNVISIS, 1982], show evident consequences of the Caríaco 1997 earthquake in the maximum horizontal acceleration distribution (Figure 5.3).

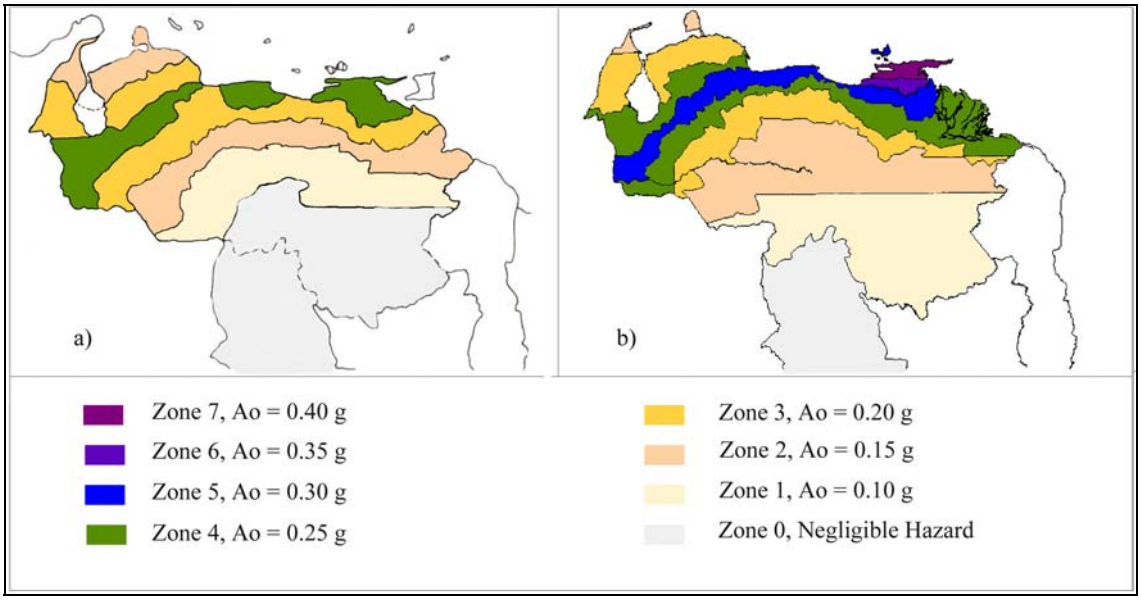

Figure 5.3: National Seismic Code comparison: a) Norma Covenin 1756-98, b) Norma Covenin-Mindur-Funvisis, 1756-82 (actual code).

Northeastern sector of the country with a previous maximum horizontal acceleration $A_0 = 0.30$ g has been divided into two zones: southerly sector (Zone 6 in present code) with $A_0 = 0.35$ g, and northerly sector (Zone 7 in present code) with $A_0 = 0.40$ g. General seismic zones division for Venezuela increased from five seismic zones in the previous code, to eight in the present one. Horizontal maximum accelerations have not changed for the first five zones, and two

new accelerations have been included for the sixth and seventh. Comparison of the historical seismicity map (Figure 5.1) with the seismic zoning maps in the codes (Figure 5.3), evidences sensitivity of the code to the July 1997 Caríaco earthquake, even though maximum Macroseismic intensity for Cumaná and Caríaco according to (Schwarz et. al, 1998) was ***I*** (MMI) = VIII. This sensitivity may be explained as the results and conclusions of post-earthquake field missions evaluating aftershock events, and updating attenuation laws for accelerations in the region with up-to-date technology and approaches. The code prior to 1997, has great resemblance with the historical seismicity map, and this may be due to the non-occurrence of an event of destructive nature since the Caracas July 09, 1967 earthquake; which also was assessed with the technology available in the late 60‘s.

5.3 Seismicity for Mérida City

Seismicity studies in Mérida require the identification and characterization of several seismogenic sources in Northwestern Venezuela. This region, for study purposes, is identified as a rectangular area located between coordinates West 68º to 74º and North 6º to 13º, where important seismicity, from different faults and fault systems exist. Historical seismic events are located inside this rectangle; the most important event is the 1812 earthquake. Its estimated intensity was IX, generating around 20,000 people dead, devastating major cities from the southwest limits (Táchira) to the coast (Caracas) and crossing through the Andean Mountains, the Falcón Basin and the Central Coastal Mountains. Chronicles describe major damages in cities in the Andean and Coastal Mountain chains, with big undamaging tremors in intermediate locations.

5.3.1 Geotectonic setting and seismicity for Northwestern Venezuela

Northwestern Venezuela includes important geographical accidents, such as the Andean Mountain Chain (in Colombia and Venezuela) and the Perijá Sierra, the valleys and sierras of Falcón and Lara States as well as the Paraguaná and Guajira peninsulas. Important seismic zones for NW Venezuela are identified [MOP, 1976]; maximum historic and instrumental records are shown in Table 5.2.

As observed, the Boconó Fault Zone (BFZ) has the maximum magnitude for historic events from all seismic zones. Restricting the analysis to a 100 km radius circle around Mérida City some authors [Rengifo, 1982; Laffaille, 1996] identify several active faults. These represent the nearest possible seismogenic sources for earthquakes in the study region due to its activity and distance to Mérida; in Table 5.3, sources, distances to the city, maximum magnitudes and maximum intensities are shown. Both studies conclude that occurrences of events with magnitudes $M \geq 5.5$ are related to the principal trace of the Boconó Fault.

Differences in the values of maximum magnitudes for the BFZ between the two tables is due to the fact that the authors considered different empiric relations to calculate magnitudes from historical data collected. However, both tables coincide in locating the maximum intensity and magnitude in the Boconó Fault Zone. The latter may be also observed in Figure 5.1, and in Map 5.2, where seismic events are condensed over the BFZ trace, determining a high seismicity region.

Other studies recognize the BFZ as the most active and important seismic source in the region, [Pérez et. al., 1997] and [Garciacaro, 1997] state that this fault zone concentrates approximately 80 percent of the total seismicity in Northwestern Venezuela and Southwestern Caribbean, occurring between 1983 and 1995.

Seismic Zone	Maximum Historic Magnitude	Maximum Instrumental Magnitude
Ancón	6.1-6.25	5.1
Arismendi	6.25	6.25
Boconó	7.3	6.88
Bucaramanga	7.3	6
El Pilar	6.8	6.8
Maracaibo	5.5	Unknown
Oca	6.1	4.5
Perijá	7.2	7.2

Table 5.2: Seismic Zones in Northwestern Venezuela (MOP, 1976).

Source	Distance (km)	Magnitude	Intensity
Boconó	12.5	8	IX - X
Granates	15	6.9	VII - VIII
Celoso	25	6	V - VI
Soledad	40	6	V - VI
Piedmont	35	6.9	VI - VII
Icotea	45	< 6.0	V

Table 5.3: Seismogenic Sources for Mérida City (100-km radius) [Laffaille, 1996].

Pérez et. al., (1997) considered a limited study area (8º – 15º N; 67º – 75º W) using precisely located micro-earthquakes occurring from 1983 to mid-1995. Figure 5.4 shows the seismicity for the region: small circles are events with $mb \geq 3.0$, open circles determine events with focal depths $h < 50\ km$, and closed circles events with focal depths $h \geq 50\ km$. Larger circles are shocks with $mb \geq 4.5$ reported in the International Seismological Center (ISC) and FUNVISIS bulletins for the period 1970 mid-1995. Solid lines are faults showing activity during Quaternary times, and triangles are seismological stations belonging to the National Seismological Network. Composite focal mechanisms (CFMS) on both the main trace of the Boconó Fault (BF) and on the sub-parallel secondary faults show a NE oriented right-lateral strike-slip motion (RLSS), and in the Andean piedmonts show NE striking reverse faulting (CFMS numerated 1 to 4, while RLSS are numbered 5 to 9).

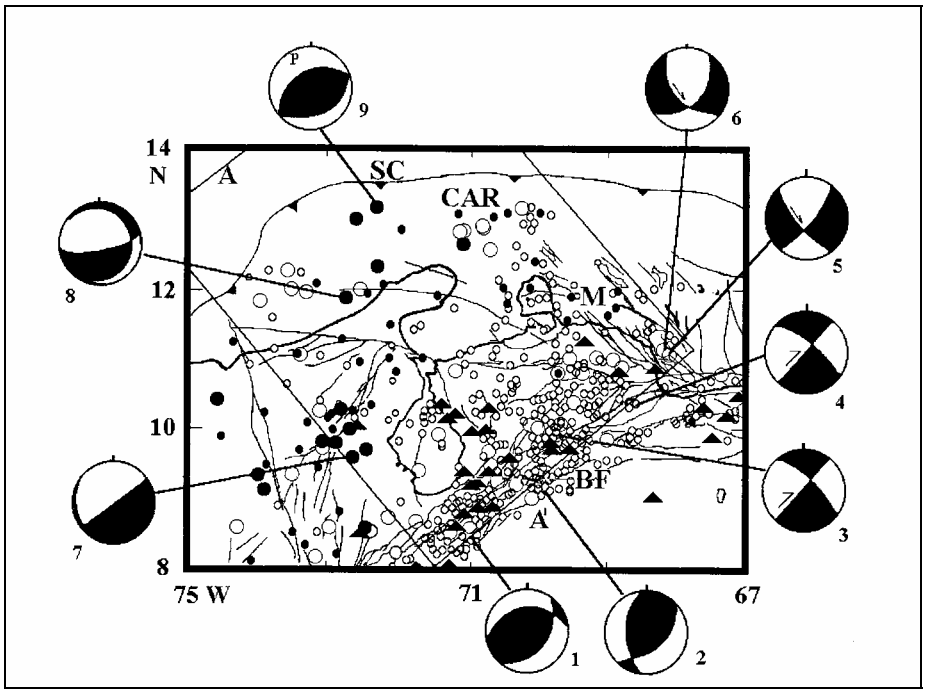

Figure 5.4: Microseismicity (*mb* ≥ *3*) in Northwestern Venezuela for period: 1983 – mid-1995 [Pérez et. al., 1997].

The largest concentration of seismic activity is observed in the stripe considered as the Boconó Fault Zone; a view of a vertical section (A – A') NW – SE oriented (perpendicular to the BFZ) in the region is shown (Figure 5.5). The same microseismic data than in Figure 5.4 has been used. Circles represent earthquake hypocenter locations, open circles are events with $mb \geq 4.5$, reported in ISC bulletins (1970 – 1982) and closed circles correspond to events reported in the National Seismological Array (1983 – mid-1995). Single arrows show orientation of the two ***T*** axes (downdip) inferred from focal mechanisms 7 and 8 in Figure 5.4, double arrows indicate shallow thrust faulting inferred from mechanism 9 from the same figure. The inclined dashed line shows the slope of the Benioff zone southwest of the study region.

These considerations highlight that BFZ is the most important seismogenic source of Western Venezuela. Its important seismicity as well as the records for the largest earthquakes in this region since 1800 (including a great rupture in 1812) determines its relevance.

The presence of a subduction mechanism of the Caribbean plate under the South American has been inferred by [Pérez et. al., 1997] with a tectonic model where the RLSS (Right Lateral Strike Slip) Boconó Fault Zone plays a major role in this multibranched plate boundary, *"...subduction of the Caribbean seafloor beneath northwestern Venezuela terminates in the vicinity of a series of NW trending faults, collectively termed Morrocoy fault zone... occurring between the northeastern tip of the subduction NW of Curaçao Island and the northeastern end of the Boconó fault zone, where it turns out to be the western end of the E-W oriented, RLSS San Sebastián fault zone along the Venezuelan coast..."*. In Figure 5.6, a schematic illustration for the plate tectonic framework of the Southwestern Caribbean-Northwestern Venezuela region is shown. Plates are: CAR, Caribbean; NAZ, Nazca; SOAM, South American; VLA, Venezuela; COL, Colombia; C, Curaçao Island. Known major fault zones are shown in thick lines where BF, MF and SF are the Boconó, the Morrocoy and the San Sebastián Fault Zones respectively, OF and SMF are the Oca and the Santa Marta Faults. Thick dashed lines in Northwestern Venezuela determine the depth contours of the upper surface for the inclined slab dipping to the southeast.

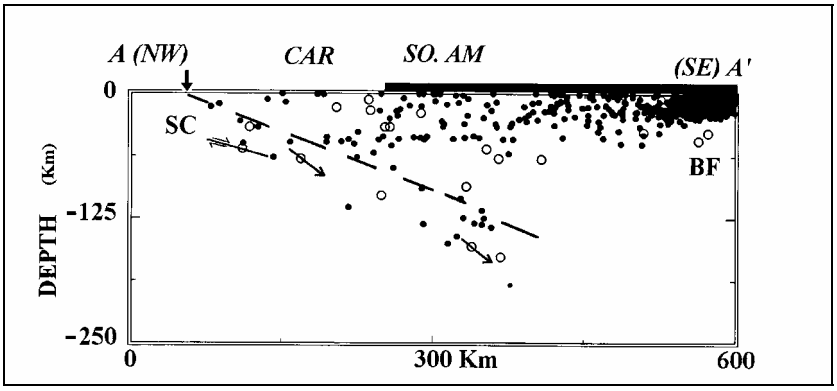

Figure 5.5: Vertical Section A – A' [Pérez et. al., 1997].

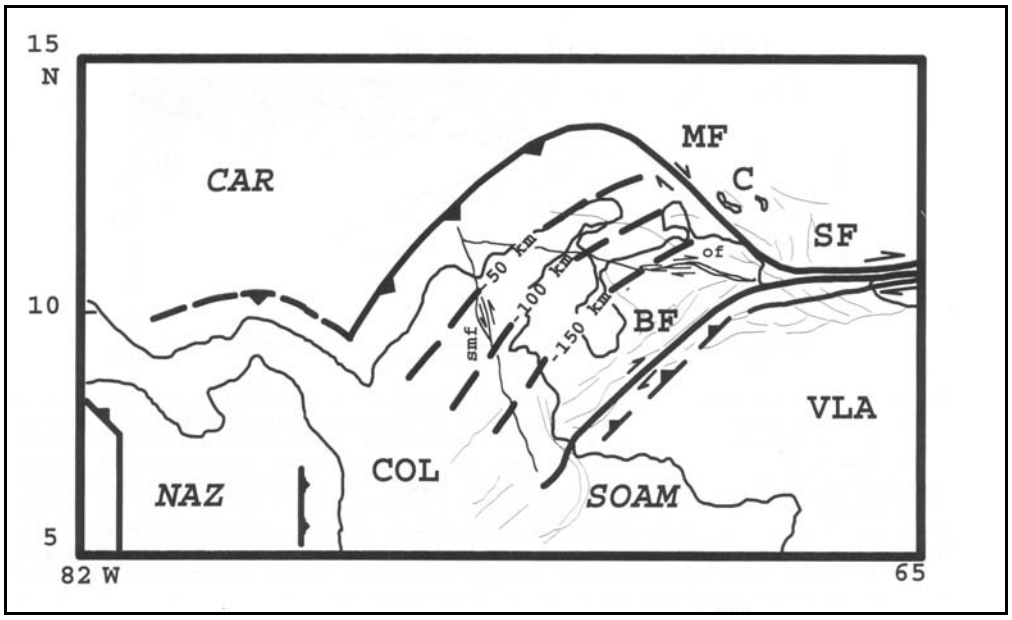

Figure 5.6: Scheme of the Southwestern Caribbean – Northwestern Venezuela tectonic framework [Pérez et. al., 1997].

In [Bendito, 2000] fourteen seismogenic zones are identified and delimited with geologic evidence; by means of seismicity analysis through the spatial variations in the Guttemberg-Richter magnitude recurrence parameters *a* and *b*, based in a proposed methodology by [Wiemer and Wyss, 1997]. In Map 5.1, seismogenic zones are shown, with the respective tectonic features in the region corresponding to the Venezuelan Neotectonic Map [Beltrán, 1993]. The most important geologic faults described include the Boconó Fault Zone, concentrating the major portion of seismicity for Western Venezuela, the Valera fault, the Oca and the Ancón Fault Zone, the Western Piedmont Fault and the Santa Marta-Bucaramanga Fault Zone in Colombia.

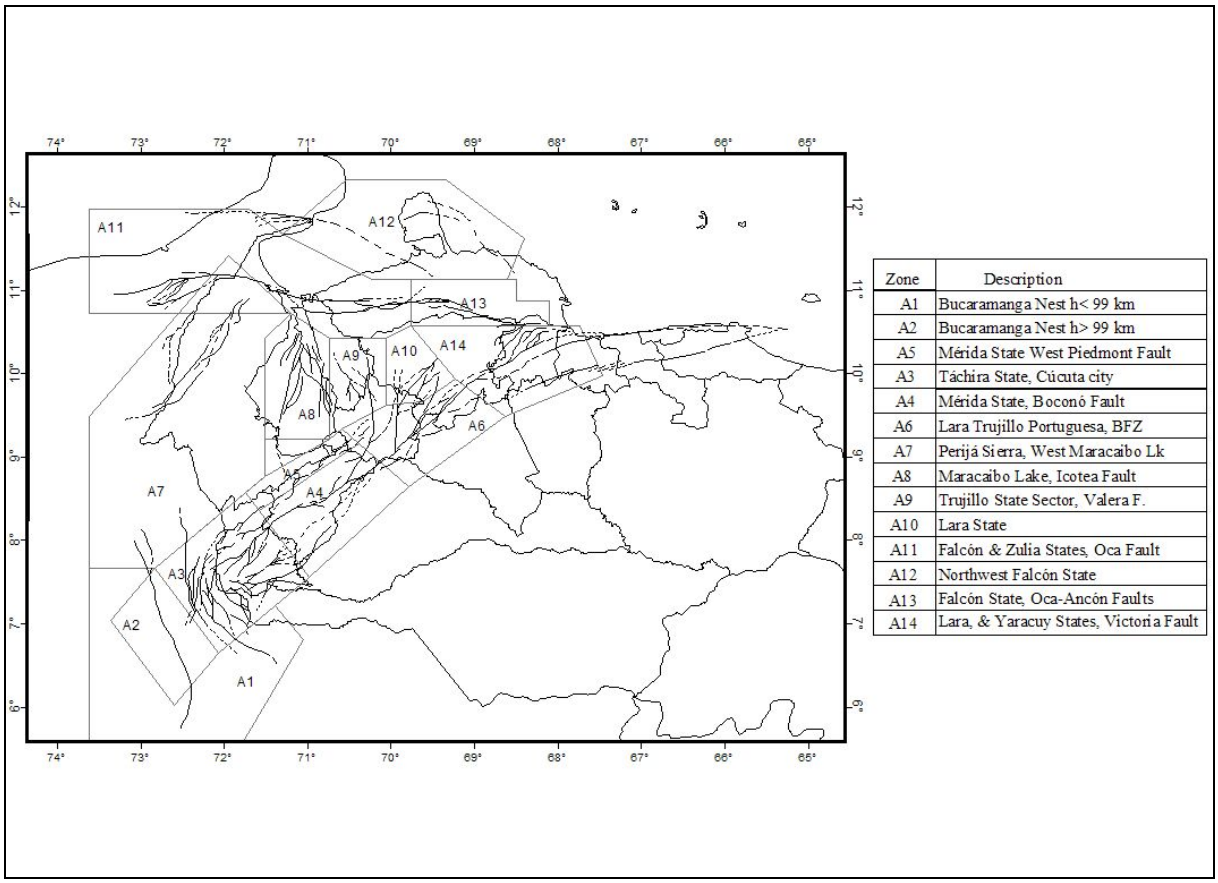

Zone	Description
A1	Bucaramanga Nest h< 99 km
A2	Bucaramanga Nest h> 99 km
A5	Mérida State West Piedmont Fault
A3	Táchira State, Cúcuta city
A4	Mérida State, Boconó Fault
A6	Lara Trujillo Portuguesa, BFZ
A7	Perijá Sierra, West Maracaibo Lk
A8	Maracaibo Lake, Icotea Fault
A9	Trujillo State Sector, Valera F.
A10	Lara State
A11	Falcón & Zulia States, Oca Fault
A12	Northwest Falcón State
A13	Falcón State, Oca-Ancón Faults
A14	Lara, & Yaracuy States, Victoria Fault

Map 5.1: Fault Zones and Fault Traces in Northwestern Venezuela (after [Bendito, 2000]).

From the historical catalog available in [MOP, 1976], between years 1610 and 1950, eighteen events with inferred magnitude Richter $M > 6.0$ are selected. Map 5.2 shows these events with their seismogenic sources identified in [Bendito, 2000]. The location of earthquakes throughout the region clearly identifies the influence of the BFZ in strong historical events. Among these, eight destructive earthquakes strongly affected cities and towns in the Andean Region; in the following, a compilation of their effects (from available historical data) is presented.

- 1610, February 03: fifty two years after Mérida's foundation, this earthquake destroyed the cities of Mérida and La Grita. The epicenter for this event was in the Western Andean Piedmont (Maracaibo Lake direction) located between the two cities. Maximum intensity inferred is *I* (MMI) = X. Sixty deaths were produced in both locations. Subterranean noises were heard days before the impact, also descending temperatures, muddy waters in wells and momentary damming of rivers and gulches were observed [Lares, 1894; Cordero, 1931; MOP, 1976].
- 1644, January 16: great damage in Mérida, Táriba, San Cristóbal and Trujillo. The epicenter was located in Pamplona (Colombia) where major damage occurred with an inferred intensity *I* (MMI) = X. This big earthquake was also felt in Cuenca, Ecuador [Cordero, 1931, MOP, 1976].
- 1812, March 26: "The great Caracas Earthquake". The cities of Caracas, Barquisimeto, San Felipe and Mérida were destroyed; the earthquake was felt in an extended region, from Caracas to Santa Marta and Bogotá in Colombia. Maximum intensity was inferred as *I* (MMI) = X in Barquisimeto and San Felipe, both cities were destroyed and the death toll rose to more than 7,000. In Caracas and La Guaira,

intensity *I* (MMI) = VIII to IX was estimated, where around 50% of houses were destroyed, and the rest were inhabitable; churches, convents and military forts were destroyed, generating more than 10,000 casualties. In mountains around Caracas (Avila Mountain and others) great cracks (surface breakage) and landslides were observed and from the Guaire River (in Caracas), black fetid water flowed downstream for some days. In the city of Mérida, *I* (MMI) = IX was inferred, most of the houses were destroyed, almost all churches and convents collapsed or suffered great damage, generating more than 800 people dead in the city. This last quantity of dead people is different from that in Table 5.1, which counts casualties (dead and injured) for all Mérida State. This earthquake was followed by a great number of seismic events until mid 1813. The great mortality generated by this event relies in the fact that March 26 was Thursday in the Easter catholic celebration and many people died trapped inside the churches [Cordero, 1931; Centeno-Graü, 1969; MOP, 1976].

- 1834, August 12: Santo Domingo town (50 km north from Mérida) was destroyed as well as other towns located in the Andean Range. Maximum assigned intensity is *I* (MMI) = VIII - IX. Although damage was localized around Santo Domingo and neighboring towns, this earthquake was felt in Mérida causing many wounded because of panic in the Clarisas Convent Church, where a mass in honor to Saint Clara was being celebrated [Lares, 1894; MOP 1976].
- 1849, February 26: Lobatera town in Táchira State was destroyed and many other neighboring towns suffered damage, with a maximum intensity *I* (MMI) = IX. Forty people dead and many wounded were generated. The earthquake was strongly felt in Maracaibo [Lares, 1894; MOP, 1976].
- 1870, June 26: at 11:00 AM, an earthquake struck El Tocuyo, with more than 30 houses destroyed and damage in roofs for most of the buildings. Assigned intensity is *I* (MMI) = VIII, 3 casualties and many wounded were produced. This day, more than 22 tremors were felt in locations near the Andean and Coastal Ranges [Centeno-Graü, 1969; MOP, 1976].
- 1875, May 18: an earthquake strikes the western part of the Andean Range, destroying around six towns in the Colombian-Venezuelan frontier; the city of Cúcuta (in Colombia) and the neighboring town of San Antonio (in Venezuela) were destroyed, with a maximum intensity ***I*** (MMI) = X - XI, casualties in Colombia were around 2,500 and in Venezuela around 350, number of wounded was not accurately recorded. Generation of cracks in soil (surface breakage) was observed in towns of the Táchira State (Venezuela) and the Santander Departament (Colombia), also some rivers dried [Cordero, 1931; Centeno-Graü, 1969; MOP, 1976].
- 1894, April 28: at 10:15 PM, a great earthquake struck Mérida and the surrounding towns of Santa Cruz, Zea, Mesa Bolívar, Tovar, Lagunillas and Chiguará. Discriminating casualties among these were: Mérida: 4; Santa Cruz: 115; Zea: 69; Mesa Bolívar: 51; Tovar: 50; Lagunillas: 21 and Chiguará: 9. Wounded raised to 30, distributed equally between Mérida and Chiguará, in other places no records for wounded were available. Maximum assigned intensity is ***I*** (MMI) = X - XI. This strong event was felt in Caracas and Bogotá (Colombia). Epicenter may be located in the Andean Piedmont at the Onia River valley, where great surface breakages and dislocations, and ejection of gases, mud and oil were observed. Great landslides occurred in hills and during the three consecutive days of the earthquake a dense cloud of dust climbed by the Chama River canyon traveling over Mérida. Water on rivers flowed with a mixture of mud and vegetation for more than one month and light radiation was observed at the SW horizon of Mérida the night of the major shock.

More than 116 tremors were felt between April 28 and August 4 that year [Lares, 1894; Cordero, 1931, MOP, 1976].

All references cited above support the existence of an important tectonic activity with relevant seismicity in Northwestern Venezuela, where historical events with important damaging effects identify the most powerful seismogenic zone as the Boconó Fault Zone (BFZ) in the region. Distances of these earthquakes to Mérida city (from 15 to 300 km) may be observed (Map 5.2) in a concentric circle array around the city, with 100 to 300 km radius at 50 km intervals. Inside the first circle (100 km radius), three of the six events with $M \geq 6.0$ within all 18 records are located, corresponding to the 1610, 1812, and 1894 earthquakes, at average distances of 70, 16, and 60 km to Mérida city, respectively. Within a 250 km radius, five of the six events described above are included.

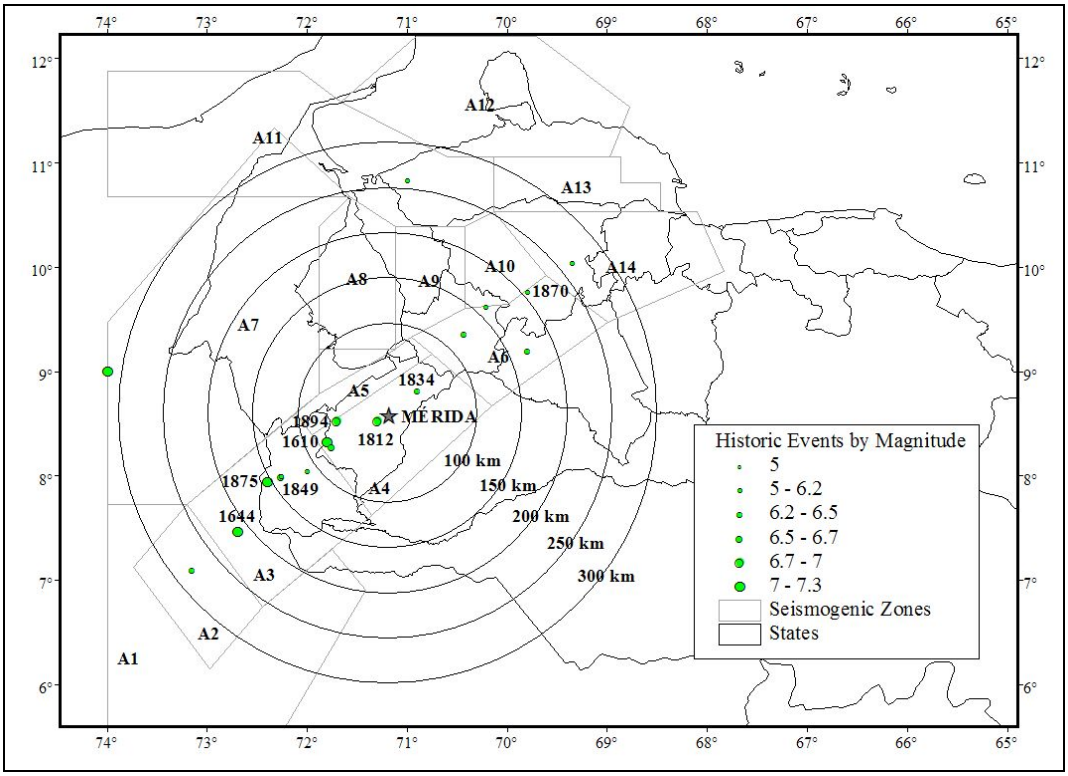

Map 5.2: Historical Events for Northwestern Venezuela.

The Boconó Fault Zone (BFZ) has been identified as the seismogenic source for Mérida's metropolitan area. Important seismic activity is distributed through this 600-km long 100-km wide NE oriented fault zone, with about 80 percent of the seismicity occurring in the region since 1983 and important historical earthquakes. In the field, the BFZ trace is recognized by modifications produced over the terrestrial surface morphology. As it crosses through the Andean Mountain Chains, from sea level to 3600 m in altitude, the trace of the fault zone and the effects of displacement are submitted to intensive erosion, though, its geomorphologic features will not endure much (in geologic time measure). The latter implies that typical geomorphologic features of the fault represent a recent geological activity and corroborates that it is an active fault.

Particular geomorphologic features of strike-slip faults are present through all the longitude of the BFZ; these are enumerated in order of abundance, from most to least (Figure 5.7).

- Displaced River Deposit (DRD): consists of sedimentary deposits of rivers and streams through the fault trace, eventually cut and displaced by the fault.

- Thermal Water Fountain (TWF): hot water emanation usually with sulfur.
- Displaced Hill (DH): formed when the fault trace crosses a hill and displaces relatively the adjacent sides.
- Closed Depression (CD) and Open Depression (OD): consists in small collapses through the fault trace, which can be closed and in this case contain Fault Lagoons (FL) or Fault Swamps (FS), and in the contrary it can be open with drainage to the outside.
- Displaced Drain (DD): formed when the fault trace cuts the course of a river or stream and forces its direction through the trace.
- Fault Scarp (FSC): produced well by a small rising of the fault trace or a horizontal displacement of a zone of greater altitude than its adjacent through the fault, or by the differential erosion of one side of the trace. Through a scarp the fault plane's exposed rock may outcrop and show a fault polish (FP).
- Indentation (IN): cut formed by the trace crossing over a hill or a hillside accentuated by erosion. If indentation is produced over a mountain edge, it may appear as a chair shaped mountain path (CHS). When fault trace crosses through a hillside produces a fault step (FS) due to vertical displacement or erosion.
- Triangular Faces (TF): in some places of the active trace, especially those where change of orientation or fault gaps are present, relatively big depressions are formed with local vertical displacements on hillsides (triangular faces) that indicate the slip planes.
- Displaced Moraine (DM): glacial till sectioned and displaced by the fault trace.
- Fault Trenches (FT): narrow, straight and long depressions formed through the fault trace.
- Aligned Valleys (AV): product of erosion of a river flowing over the fault trace.

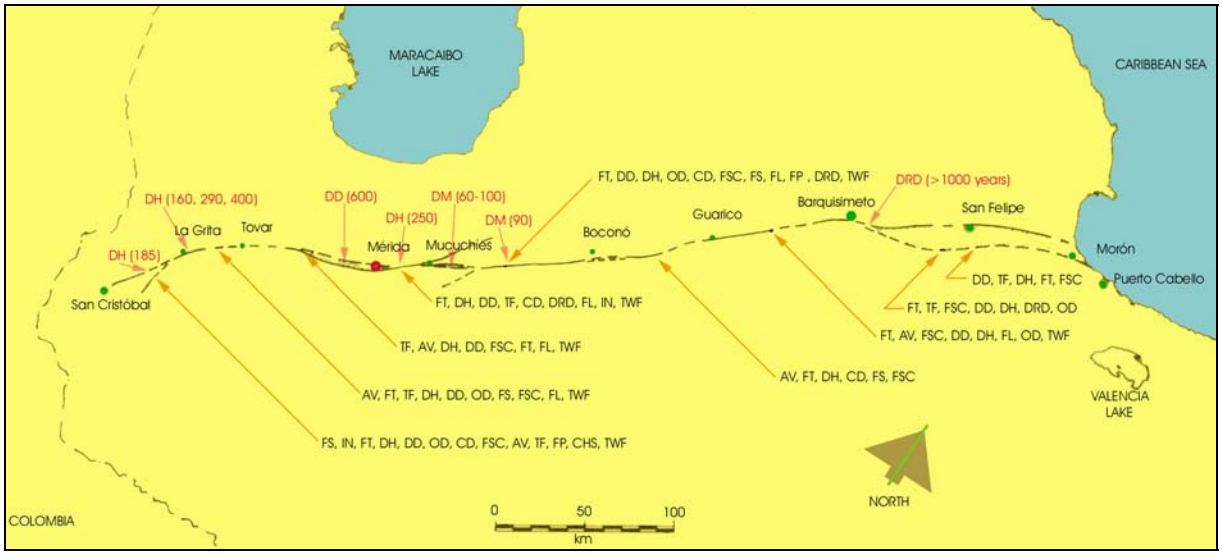

Figure 5.7: Geomorphologic features in BFZ trace, after [Schubert, 1984].

In Figure 5.7 all geomorphologic features exposed are shown in the same order through the BFZ principal trace, also the dominant features with the respective Right-lateral strike-slip (RLSS) displacements in meters are shown.

Right-lateral strike-slip (RLSS) displacements are measured through the longitude of the BFZ's principal trace (see Table 5.4). It is shown that displacements of moraines range between 60 and 250 m, the maximum age of these features is 18,000 years, then the estimated velocity of displacement varies between 0.3 and 1.0 cm/year [Schubert, 1984]. The movement through the longitude of the BFZ is not uniform. At the northern and southern limits right-lateral movement experiences a progressive decrease, reaching values of 1 mm/year in the Colombian frontier and 1.5 to 3 mm/year in its northern limit in Morón, on the other hand, movement in Central Andean sector evidences a velocity of 1 cm/year. This velocity variation may be due to movement absorption by the notorious ramifications of the principal trace, as well as to sub-parallel satellite faults [Singer and Audemard, 1997].

Displacement	Type and age of feature
100 km	Frontal-sliding displacement (Early Tertiary)
15 – 75 km	Tertiary-Precambrian rock outcropping
68 km	Frontal-sliding displacement (Early Tertiary)
65 km	Precambrian-Paleozoic rocks outcropping
50 km	Metamorphic rocks contrast (Late Mesozoic)
45 km	Cretaceous rocks displacements
40 km	Paleozoic rocks displacements
10 – 37 km	Pre-Cretaceous rocks displacements
33 km	Displaced Drains (Late Tertiary)
30 km	Metamorphic rocks contrast (Late Mesozoic)
9 km	Cretaceous rocks displacements
120 – 1000 m	Displaced River Deposit (Quaternary)
70 – 1600 m	Displaced Hills (Quaternary)
120 – 600 m	Displaced Drains (Quaternary)
100 – 400 m	Displaced River Deposit (Quaternary)
100 – 250 m	Displaced Moraines (Late Quaternary)
80 – 100 m	Displaced Moraines (Late Quaternary)
98 m	Displaced Moraines (Late Quaternary)
60 – 80 m	Displaced Moraines and Drains (Late Quaternary)
1 – 80 m	Displaced Glacial Features (Late Quaternary)
62 – 69 m	Displaced Moraines (Late Quaternary)

Table 5.4: Right-Lateral Strike-Slip movements in BFZ measured in geologic and geomorphologic features [Schubert, 1984].

5.3.2 Previous seismicity analyses for Mérida

Various authors, through different methodologies, have performed several seismicity studies for Mérida; these are briefly described chronologically with the methodology used and relevant results obtained.

- [MOP, 1976]: calculates return periods through probabilistic analysis using the Gumbel I extreme distribution over a composed catalog with data recorded between 1950 and 1971, treatment of the data was performed and catalogued by: [Sykes and Erwin, 1965] for years from 1950 to 1964 and (I.S.S. Catalog, Edinburg) for from years 1965 to 1971. Return periods for different magnitudes are shown in Table 5.5 where the most important fact is that the magnitude 8 event return period (worst expected) is around 135 years.

Magnitude	Return Period
3	20 days
3.5	59 days
4	5.8 months
4.5	1.4 years
5	4.8 years
5.5	8 years
6	15 years
6.5	25 years
7	45 years
7.3	62 years
7.5	77 years
8	135 years

Table 5.5: Return Periods for Mérida City [MOP, 1976].

- [Rengifo, 1982]: a probabilistic seismic hazard analysis (PSHA) is performed based in the Guttemberg-Richter recurrence law over a 100 km radius zone around Mérida, and an observation period from 1900 to 1980. Data fit for recurrence law has the form:

$$\log N = 4.66 - 1.02M \qquad \text{eq. 5.1}$$

  Return periods obtained from this law are shown in Table 5.6, where maximum expected magnitude has a return period of 300 years.

Magnitude Range	*N*	Return Period (years)
M ≥ 4	4.054	0.26
M ≥ 5	0.327	2.7
M ≥ 6	0.037	28.6
M ≥ 7	-	300

Table 5.6: Return Periods for Mérida [Rengifo, 1982].

- [Laffaille, 1996]: based in a deterministic approach (DSHA), this author identifies eight seismogenic sources (see Table 5.3), and by historical and instrumental records identifies scenario events for each of the sources. In this research the 1812, M = 8 Richter, $\boldsymbol{I}$ (MMI) = X event is established as the scenario earthquake for Mérida city, associated to the Boconó Fault Zone as the seismogenic source.
- [Garciacaro, 1997]: deterministic approach (DSHA), by means of displacements over the principal trace of the BFZ (~ 1.0 cm/Year), and the maximum expected rupture, compared to that occurred in the 1812 earthquake, supposed to be 2.5 meters in total longitude. Based in these facts, the return period for an event of this nature is calculated as ~250 years; establishing consequently, a very high seismic risk level for the Venezuelan Andean region.

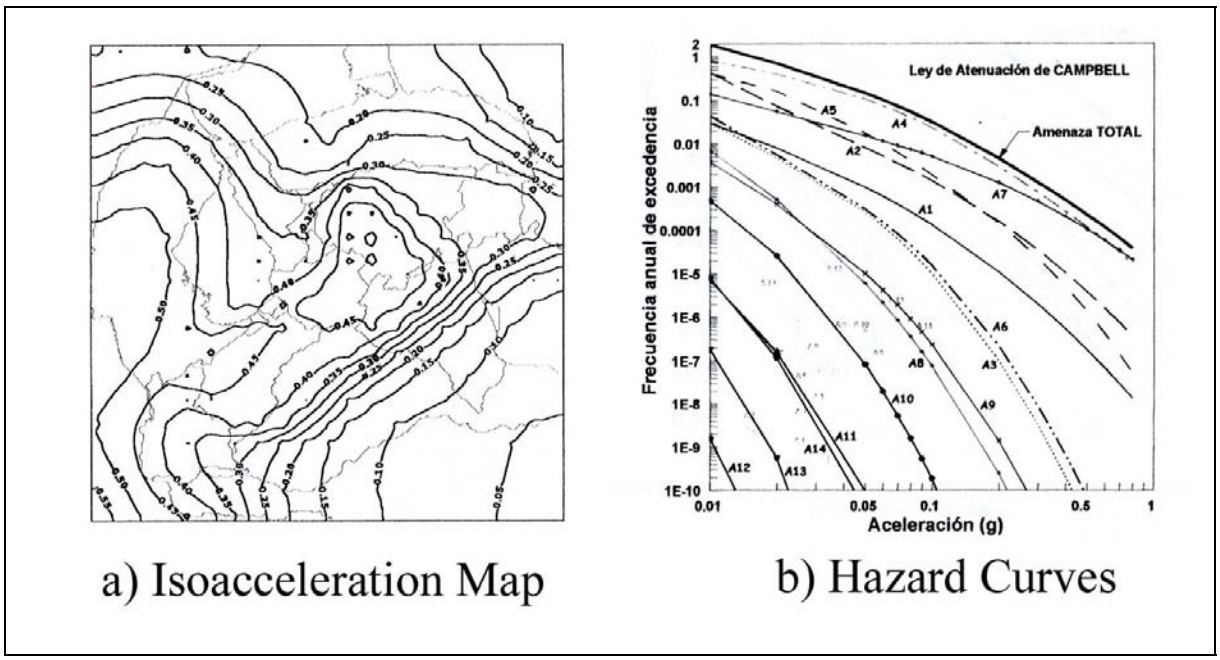

Figure 5.8: Isoacceleration Map for Western Venezuela and Hazard Curves for Mérida City [Bendito, 2000].

- [Bendito, 2000]: performs a probabilistic seismic hazard analysis (PSHA), over fourteen identified seismogenic zones, based in bounded Guttemberg-Richter recurrence laws, for a catalog based in several national and international databases; establishing hazard curves for each of these zones. The deaggregation of accelerations is also performed to obtain isoacceleration curves for Northwestern Venezuela based in four performance states for the structures. A compound of isoacceleration map and

hazard curves for Mérida city for a 970 years return period are shown in Figure 5.8 a) and in Figure 5.8 b), respectively; the highest hazard curves are generated by the Boconó Fault seismogenic zone (A4), with the greater accelerations over Mérida's location.

5.3.3 Seismic hazard analysis in Mérida

A non-zonified probabilistic seismic hazard analysis through the Gumbel III extreme values distribution is performed over a rectangular zone with UTM coordinates W 68º to 74º and N 6º to 13º, considered as Northwestern Venezuela. Data for analysis corresponds to instrumental records available from several sources: [MOP, 1976] with data from 1950 to 1971, [USGS, 2001] with data from 1950 to 2001 and [REDSAV, 2001] with data from 1989 to 1999.

The selection of events is performed through comparison of databases for overlapping years, eliminating repeated events in [USGS, 2001] as the other two databases are considered more reliable due to its use in previous catalogs for the region. A total number of 2,195 events covering the period 1950-2001 are collected in a single compound database to be used in this analysis. The data is homogenized using *mb* magnitude by the relationships for Venezuela [GSHAP, 1998], general forms for these relationships are:

$$Ms = 1.116mb - 1.067, \quad for\ mb \le 5.8 \qquad \text{eq. 5.2}$$

$$Ms = 2.741mb - 10.369, \quad for\ mb > 5.8 \qquad \text{eq. 5.3}$$

The maximum magnitude observed in the data is $mb = 6.5$ with one event, and the minimum is $mb = 2.0$, nevertheless, for extreme values analysis, only maximum events are taken into consideration, and for this dataset threshold magnitude for lower boundary is proposed as $mb = 4.0$. Following the procedure for parameters estimation in Section 2.4.2.2, for the Gumbel III analysis, the fit for the distribution function is performed obtaining the best correlation based in shape factor $\boldsymbol{k}$ (with the data used) as the other parameters ($\boldsymbol{\omega}$, $\boldsymbol{u}$) for the fit are fixed as upper and lower bounds respectively. (see eq. 2.13). Parameters for best-correlated fit for distribution function are: upper limit $\omega = 6.5$, lower limit $u = 5.4$, and shape factor $k = 3.6$, obtaining a correlation factor (through expressions 18. and 19.) of 0.99035, the function has the general form:

$$F_Y(y) = \exp\left[-\left(\frac{6.5 - y}{6.5 - 5.4}\right)^{3.6}\right] \qquad \text{eq. 5.4}$$

Exceedance probabilities are estimated over periods of one (1), 30, 50, and 100 years. In Figure 5.9, results for annual exceedance probabilities and return periods are shown. Ground motion parameters (macroseismic intensities and ground surface accelerations expected) are assessed by attenuation laws (both related to magnitude of events) in order to determine the probabilities and expected levels of accelerations for the different intensities.

Macroseismic intensities estimation through an attenuation law is used to establish the different probable levels for seismic events. In this research, the Macroseismic scale used is the European Macroseismic Scale [EMS, 1998]. Threshold for damage occurrence is $I(EMS) = VI$, defined as "Slightly Damaging"; subsequent levels of the scale and its equivalence to magnitude are estimated, considering the shortest hypocentral distance of 15 km for an event in the Boconó Fault Zone. The attenuation law available is that of [Aggarwal, 1981], obtained by isoseismic curves relationships for some historic events occurred in the Venezuelan western region, general form is:

$$I(R) = 2.98 + 1.5M - 1.70 \ln R \qquad \text{eq. 5.5}$$

Where, R is the hypocentral distance (km) and M is the M_S magnitude. This relationship presents attenuation starting at a hypocentral distance of 14 km.

For ground acceleration levels expected, several attenuation laws are available from different national and international research groups and institutions. General equation for the laws is:

$$\ln a = A + BMs + C \ln(R + D) \qquad \text{eq. 5.6}$$

Where, a is the ground acceleration in *gals*, R is the hypocentral distance (km) and M is the M_S magnitude.

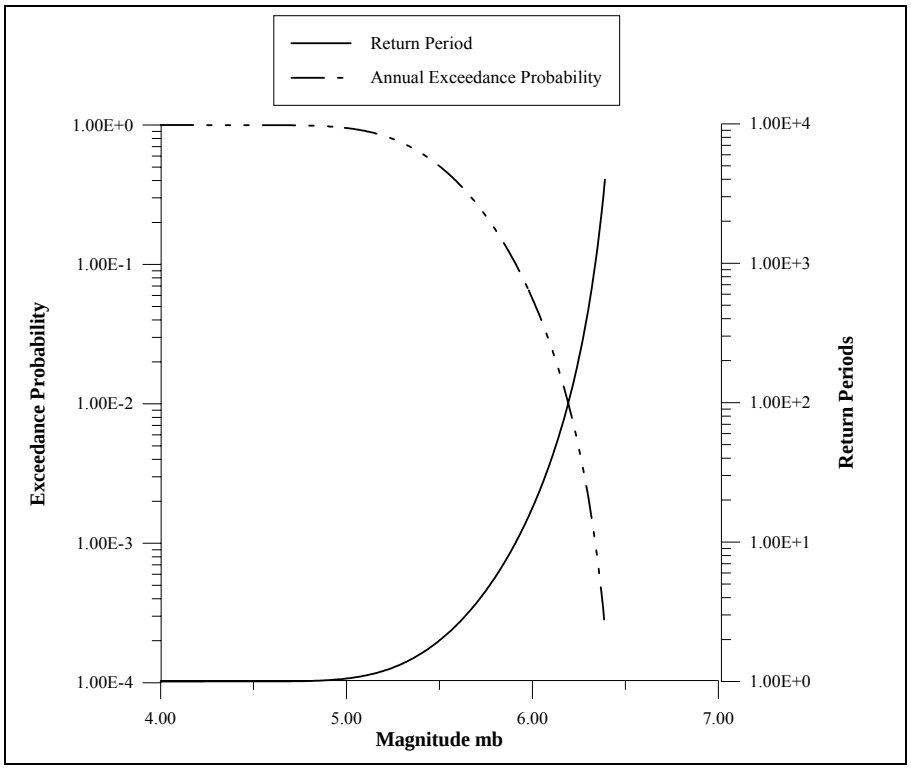

Figure 5.9: Annual Exceedance Probabilities and Return Periods for Magnitudes.

The attenuation laws for Venezuela are not directly inferred from acceleration records, due to the unavailability of a significant number of records; thus, relationships are established through local intensity estimations and acceleration records from other places in the world. In [Malaver, 2000], a comparison for different attenuation laws and acceleration records available for Venezuela is performed, the study evaluates by means of the regression: $\sum(Ar - Ap)^2$ the best fit between recorded and predicted accelerations (Ar and Ap, respectively), results are shown in Table 5.7, where the INTEVEP (Nº 1) attenuation law represents the best fit for data. The first four laws were obtained in Venezuela, using local intensity estimations, for Nº 1 and 2, and world acceleration records in rock or firm soil for Nº 3 and 4. The remaining laws (Nº 5 and 6) were performed based in records from the U.S. West Coast.

Based in the results of Gumbel III probabilistic analysis, and by the use of the INTEVEP attenuation law, four events may be selected ranging from intensities VI (Slightly Damaging) to IX (Destructive). Capability of considering an intensity X (Very Destructive) earthquake is out of the range of this probabilistic analysis; it would be necessary the occurrence of an

$Ms = 7.7, mb = 6.7$ event, but the largest considered in the data is an $Ms = 7.0, mb = 6.5$ event. In Table 5.8, results for the estimation of the probabilities and return periods for expected maximum horizontal acceleration levels (in fractions of gravity acceleration) corresponding to different intensities are shown. These four scenario earthquakes are the ones selected for risk analysis throughout this research. In Table 5.8 the return period for the I = VI event is 2 years, which may be considered as undervalued, as in the last 10 years only one event of this power (M = 5.1) has occurred in the delimited zone of study and a total of three events are observed in the database for probabilistic analysis. Thus, the seismic hazard estimated for moderate events seems to be overvalued, i.e. the return period for these events are expected to be greater than 2 years.

Nº	**Law**	*A*	*B*	*C*	*D*	$\sum(Ar - Ap)^2$
1	INTEVEP [Quijada et. al., 1993]	5.40	0.36	-0.86	10	0.0194
2	FUNVISIS [Dragone et. al., 1984]	4.87	0.96	-1.56	25	0.0272
3	WDC [Cascante, 1988]	4.402	0.48	-0.74	0	0.0255
4	CORAL 83 [Coral 83, 1991]	4.86	0.51	-1.00	5	0.0223
5	J & B [Joyner and Boore, 1988]	5.998	0.398	-1.23	0	0.0368
6	McGÜIRE [McGuire, 1976]	7.089	0.484	-1.3	25	0.0219

Table 5.7: Attenuation laws for Venezuela [Malaver, 2000].

Intensity (EMS)	**Magnitude (Ms)**	**Maximum Acceleration (g's)**	**Annual Exceedance Probability**	**Return Period (Years)**
VI	5.1	0.089	0.4705	2
VII	5.8	0.1147	0.0743	13-14
VIII	6.4	0.1422	0.0117	86
IX	6.8	0.1646	0.0012	831

Table 5.8: Scenario Earthquakes for risk analysis.

5.4 Microzonation studies in Mérida city

Microzonation studies provide information on possible local and induced effects (e.g. amplification, liquefaction and landsliding) for soils due to the action of a specific seismic

event. The range of possibilities depends on seismicity patterns (power and recurrence) and local site response (expected acceleration levels) for specific soil conditions (geologic, topographical and geotechnical features).

5.4.1 Previous Microzonation Studies and Results

In Mérida, the available Microzonation study is in [MOP, 1976]; no other complete analyses have been performed before and since then. In that study, a geophysical assessment for Mérida's plateau was performed by seismic refraction tests with wave generation through explosives and mechanical impacts. For soil layering, lineally arrayed superficial devices (geophones) were located at distances of 20 m to 50 m, with 12 geophones in total; all were performed with explosives in bore holes with depths from 4 to 10 m at the end of the devices arrays. Thirty-four seismic superficial devices were performed with 764 seismograms registered. Two parametric devices were performed at different layer outcrops to determine and calibrate longitudinal and transversal waves; techniques used were those of the Up-hole and Cross-hole methods with the use of mechanical impacts for wave generation, with a total of 120 resulting seismograms. Geologic conditions were also assessed by means of maps and site surveys; general conclusions for assessment are presented in the next section.

5.4.2 Plateau of Mérida: Geology, Geomorphology and Geotechnics.

Geologic and geomorphologic conditions: Mérida is settled in a tectonic valley (graben) with NW limits on the La Culata Sierra and SE limits in the Sierra Nevada. The valley is constituted by Alluvial deposits in cone-terrace shape (Pleistocene era), fluvial spreading and terraces. Slope in the terrain ranges from 0 to 15 grades in the central part of the valley. Three rivers cross the surface: the Chama, the Mucujún and the Albarregas rivers. The first separates the Pleistocene terrace (over which the city is settled) from the Nevada Sierra through a canyon with maximal depths of 180 m. The Albarregas River with a slope from 2 to 3 grades is controlled by faults, as it may be seen in its linearity [MOP, 1976]. Slopes on the river borders depend on canyon depths and range in general from 20 to more than 40 grades.

Geologic outcroppings in the study area are:

a) Palmarito formation (Permian Carboniferous): covering approximately 20 percent of the total area and partly forming the spurs of the La Culata Sierra. Consists in laminated mudstone, clay rock, silty loam and chalk. Presents a considerable amount of unstable and sliding zones, particularly where layers dip in the same direction of the slope.
b) Consolidated NW Section (Quaternary): fluvial terraces of the rivers, recent debris cones and gravel-pebbles terraces, from the Pleistocene era, constitute over 50% of the studied area.

The soil composition is an extensive sedimentation of lime, sand, gravel and variable size of pebbles, which came from the sides of the Sierras in the boundaries of the valley.

The geotechnical conditions of soil and sub-soil comprises a three-layered deposit that describes the general constitution of Mérida's tableau, these are:

1) Surface zone: composed by heterogeneous material with predominant presence of fines and gravel, i.e. sand and clay with gravel and few pebbles. Velocities for longitudinal waves (V_p) range between 0.4 and 2.0 km/s, and for transversal wave (V_s) from 0.3 to 0.8 km/s. Thickness of this layer varies generally between 4 and 16 m, and in some isolated locations depths can be 18 or 20 meters. Average location of water table (groundwater) is 3 m.

2) Middle or Intermediate zone: composed by a great percentage of fractured rocks pebbles and gravel with a variable proportion of lime and sand, produced by meteorization of the Sierra Nevada formation. Generally, rough particles in a fine mesh form a compact material. Registered longitudinal wave velocity ranges from 2.1 to 2.9 km/s and transverse wave velocities are within the range of 0.8 and 1.7 km/s. Thickness of intermediate zone varies between 55 and 120 m.
3) Deep zone: contains fractured and massive rock with velocities greater than 3.0 km/s for longitudinal waves. Depth varies from 60 m to 130 m although 40 m minimal and 150 m maximal depths are present (in relatively small areas).

The Albarregas River separates two different soil constitutions for the surface zone at each side of it, in the northerly region soils are a mixed compound of clay and sand with small quantities of gravel and at south soils are composed by a mixture of sand and lime with gravel.

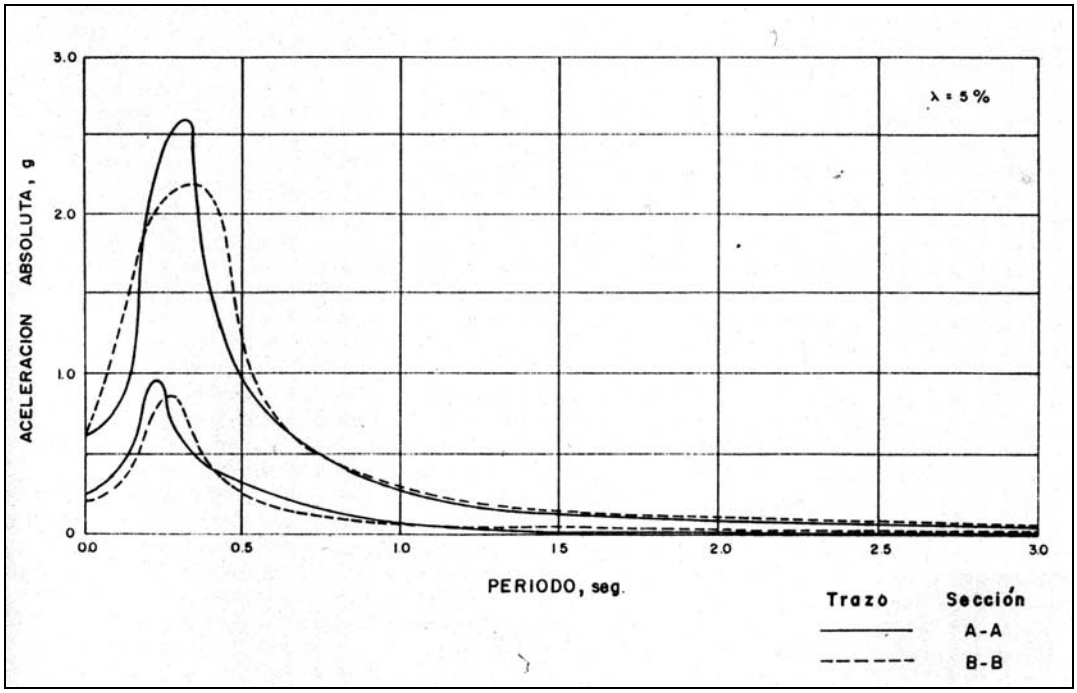

Figure 5.10: Acceleration Spectra for different soils in Mérida's Tableau [MOP, 1976].

Coming again to the previous microzonation study (MOP, 1976), site response was estimated by the use of SHAKE2 program [Schnabel et. al., 1972] with artificial and recorded accelerograms (with different magnitudes and distances to the source) as input over two different soil columns: northerly and Southerly Albarregas River. In the resulting elastic response spectra, shown in Figure 5.10, maximum amplifications occur between the period intervals 0.2 s to 0.4 s, with similar spectral shapes for both deposits; maximum values for spectral shapes in southerly region, which is represented by the Sección A- A curve in Figure 5.10, were approximately a 15% greater than in the northerly region, which is represented by the Sección B – B curve in the same Figure 5.10. No local effects were considered in that study.

5.4.3 Microzonation Analysis.

Based on data revealed by hazard analysis and data obtained from the previous study presented [MOP,1976], a further assessment is performed to obtain particular response parameters in Mérida city's soils, i.e. to estimate the probable local and induced effects such as: local amplification, liquefaction and landsliding. These phenomena are related to the geologic, geomorphologic and geotechnical characteristics of the soils in Mérida's plateau. To perform this assessment an estimation of expected acceleration levels at ground surface is required, to determine the critical accelerations for each of the local effects considered and crossing with other information pertaining specific characteristics of geologic units in the interest zone.

5.4.3.1 Site response analysis

Site response is estimated over the basis of scenario earthquakes (described in Table 5.8) and by the use of Equivalent-linear Earthquake site Response Analysis software (EERA) [Bardett et. al., 2000] which requires as input data, a geotechnical column for the soil, and an acceleration time history.

Geotechnical models for soil compositions are those of Figure 5.11. These models are those available in the SHAKE91 program [Idriss and Sun, 1992]. For materials such as: a) Alluvial Gravel, b) Clay, c) Sand and d) Rock. For soil characterization, two columns for average conditions in Mérida's tableau soils are used (Table 5.9).

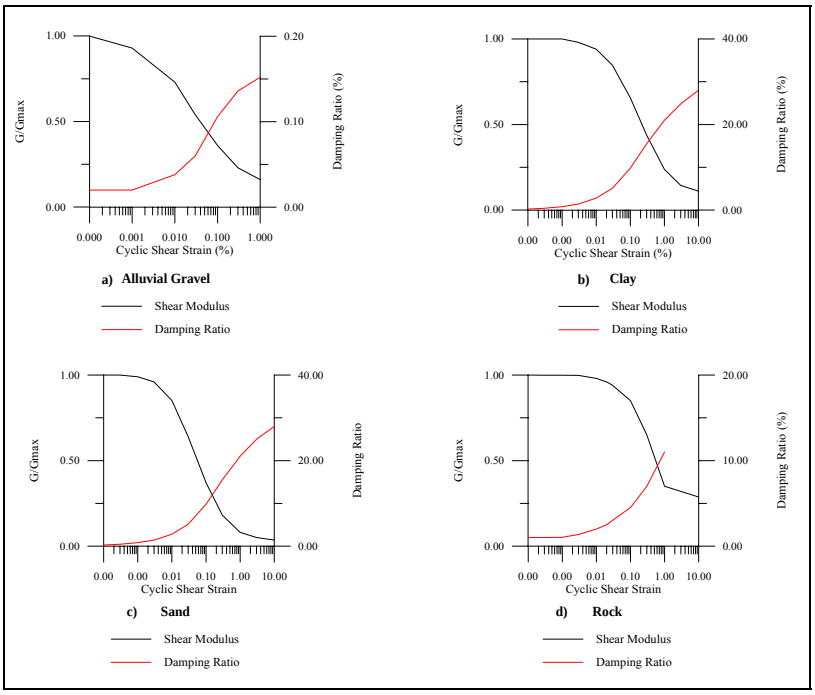

Figure 5.11: Geotechnical properties for materials used in analysis.

Acceleration time histories are obtained by the use of Target Acceleration Spectra Compatible Time Histories software -TARSCTH- [Papageorgiu et. al., 2001]. This program computes time-histories for accelerations based on elastic response spectra considered in seismic codes, depending also on event magnitude, distance to the source and the faulting mechanism. The time histories accelerations are then scaled to the maximum acceleration expected for each

scenario event. The use of the TARSCTH software is believed to be convenient due to the unavailability of enough acceleration records for Mérida's tableau, which leaves as alternative to work with the acceleration spectra and maximum expected horizontal accelerations in the Venezuelan seismic code.

Soil Type	Layer	Composition	Unit Weight (KN/m^3)	Shear Wave Velocity (m/s)
Northerly Albarregas River	Surface	Sandy Clay with Gravel	18.85	200 to 800
	Intermediate	Silty Sand with Gravel	19.64	800 to 1,700
	Deep	Boulders, Pebbles and Gravel	22.06	Over 2,000
Southerly Albarregas River	Surface	Clayey Sand with Gravel	19.64	200 to 800
	Intermediate	Silty Sand with Gravel	20.43	800 to 1,700
	Deep	Boulders, Pebbles and Gravel	22.01	Over 2,000

Table 5.9: Geotechnical Soil Columns used in Analysis [MOP, 1976].

For the case pertaining this research, elastic response spectra considered is that of the Venezuelan Seismic Code [MINDUR and FUNVISIS, 1998], which for Mérida considers a maximum horizontal effective peak ground acceleration $A_0 = 0.30\,g$ while the constant acceleration spectral response is found between $T^* = 0.7$ s and $T_0 = T^*/4$. (Figure 5.12). The resulting acceleration time histories from TARSCTH software with the respective acceleration response spectra (5% damping) are shown in Figure 5.13. The RSCTH's collection represents synthetic accelerograms corresponding to the scenario earthquakes (Table 5.8) with a fault distance of 15 km considered as the most unfavorable. The other synthetic signal: D_150 corresponds to a 6.8 magnitude event at a distance of 150 km from the source. The last record is identified as the Diamond Heights (17-10-89) earthquake accelerogram recorded at the Loma Prieta station (80 km from the source), with a maximum acceleration of 0.06 g. In all cases maximum acceleration response spectra is found around 0.2 and 0.8 s, matching the 5% elastic response spectra provided by the Venezuelan Seismic Code.

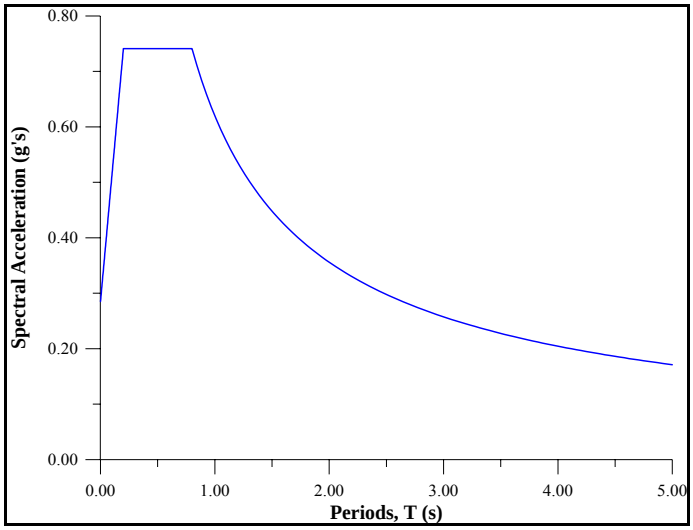

Figure 5.12: Elastic Response Spectra for Mérida [MINDUR and FUNVISIS, 1998].

Procedure for Site Response Analysis:

- Geotechnical columns: two columns are described as representative for average soil conditions depending on relative location with respect to the Albarregas River (see Table 5.9). Additional analysis is performed in columns, with different depths for the first layer to estimate changes in amplification factors and periods of occurrence. First layer depth values range from 2.0 m to 20.0 m depth with a 2.0 m step interval, resulting in twenty different geotechnical columns.
- Acceleration Time Histories: six accelerograms are used in the analysis, five synthetic and one recorded. Four out of the five synthetic signals consider scenario seismic events with distances to the source of 15 km, and one with magnitude 6.8 and a distance of 150 km to the source. Elastic response spectra considered for synthetic signals is that of Figure 5.12. A recorded acceleration time history is used, corresponding to the Loma Prieta Diamond Heights registered event. The acceleration time histories for each scenario earthquake, and the other two accelerograms considered are shown in Figure 5.13.
- Site response estimations: the six acceleration time histories described above are used for each of the twenty geotechnical columns considered, with a total of 120 site response estimations (Maximum Amplification Factor / Period) depending on first layer depths and compositions (Northerly/Southerly Albarregas River). A collection of Surface Response Spectra is obtained for every depth at all events considered.

Name of signal	Intensity (EMS)	Magnitude (Ms)	Distance (km)	PGA (g)
RSCTH1	VI	5.1	15	0.089
RSCTH2	VII	5.8	15	0.1147
RSCTH3	VIII	6.4	15	0.1422
RSCTH4	IX	6.8	15	0.1646
D-150	IX	6.8	150	0.4042
Diamond Heights	N/A	7.1	80	0.1129

Table 5.10: Geotechnical Soil Columns used in Analysis [MOP, 1976].

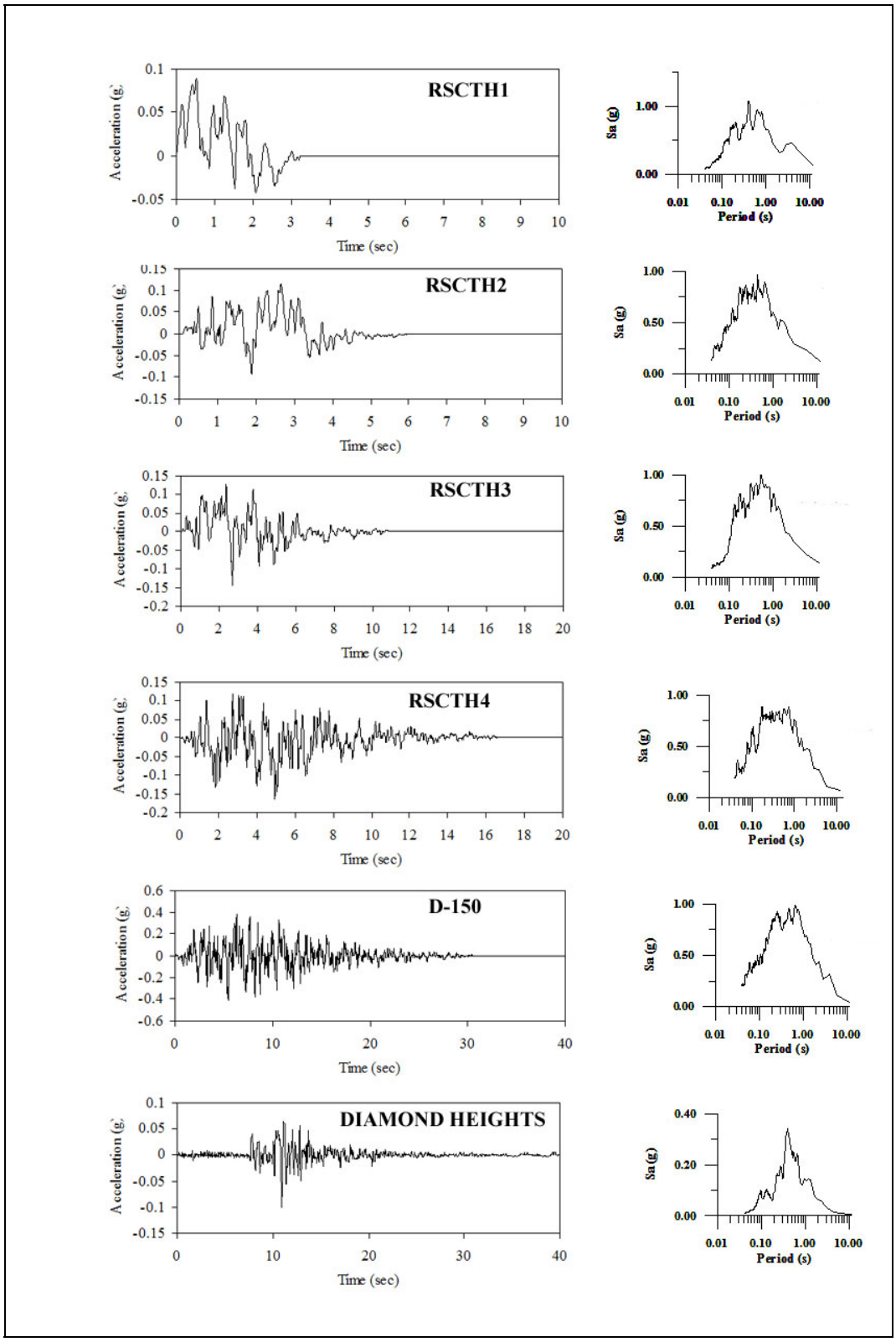

Figure 5.13: Acceleration Time Histories and Spectral Accelerations used in analysis.

Results for Site Response Analysis: results are separated into the two types of soils in Mérida's Tableau.

- Northerly Albarregas River:

- Amplification Factor (AF): Figure 5.14 shows that AF's increase with First Layer thickness increment, ranging from 2.50 to 2.85 (in average). For the first three events (Figure 5.14a, b and c) there is a decrement with a consequent slope change between 6.0 and 10.0 m thickness, continuing from this point with the same slope as the previous interval (2.0-6.0 m). For the rest of the events (Figure 5.14d, e, and f) the slope has the same sign and variation is slight. Maximum Amplification Factor occurs at 20.0 m thickness for the first layer in all cases.
- Period of Maximum Amplification (PMA): PMA's are also increasing with First Layer thickness increment. Ranging from 0.05 to 0.25 s, in general, there is a slope change and a subsequent jump to upper values (around 4 times) in PMA's that starts, for lower magnitudes at 10.0 m thickness and sets back for lower thickness at higher magnitude events until reaching 4.0 m thickness in the highest considered (see Figure 5.14).
- Average Surface Response Spectra: for each event, an average surface response spectra through all depths considered has been estimated. As it may be seen in Figure 5.16 a, synthetic signals for increasing values of magnitude have increasing maximum values in its respective response spectra at around 0.20 s, in the case of Diamond Heights record maximum value in spectra is located at 0.39 s Period. Maximum value in the Average Surface Response Spectra is 0.57 g at 0.21 s Period. Values greater than 0.30 g in acceleration is located between Periods 0.09 and 0.76 s (see Figure 5.16 c).

- Southerly Albarregas River:
  - Amplification Factor (AF): as seen in Figure 5.15 there is an AF's increase with First Layer thickness increment, ranging (in average) from 2.11 to 2.98 times the input. Maximum Amplification Factor occurs at 8.0 m thickness for the first layer in all cases except for the first scenario event, where maximum AF occurs at 6.0 m thickness. In general, after reaching maximum AF there is a decrement with the consequent slope sign change until 16.0 m depth where slope sign changes once more and AF's increase.
  - Period of Maximum Amplification (PMA): there is a PMA increase with First Layer thickness increment ranging from 0.04 to 0.25 s. In general, there is a slope change and a subsequent jump to upper values (around 3 times) in PMA'S starting for all events at 14.0 m thickness. This slope change ends at 16.0 m thickness where initial slope is recovered; PMA is maximum at 20.0 m thickness in all cases (see Figure 5.15).

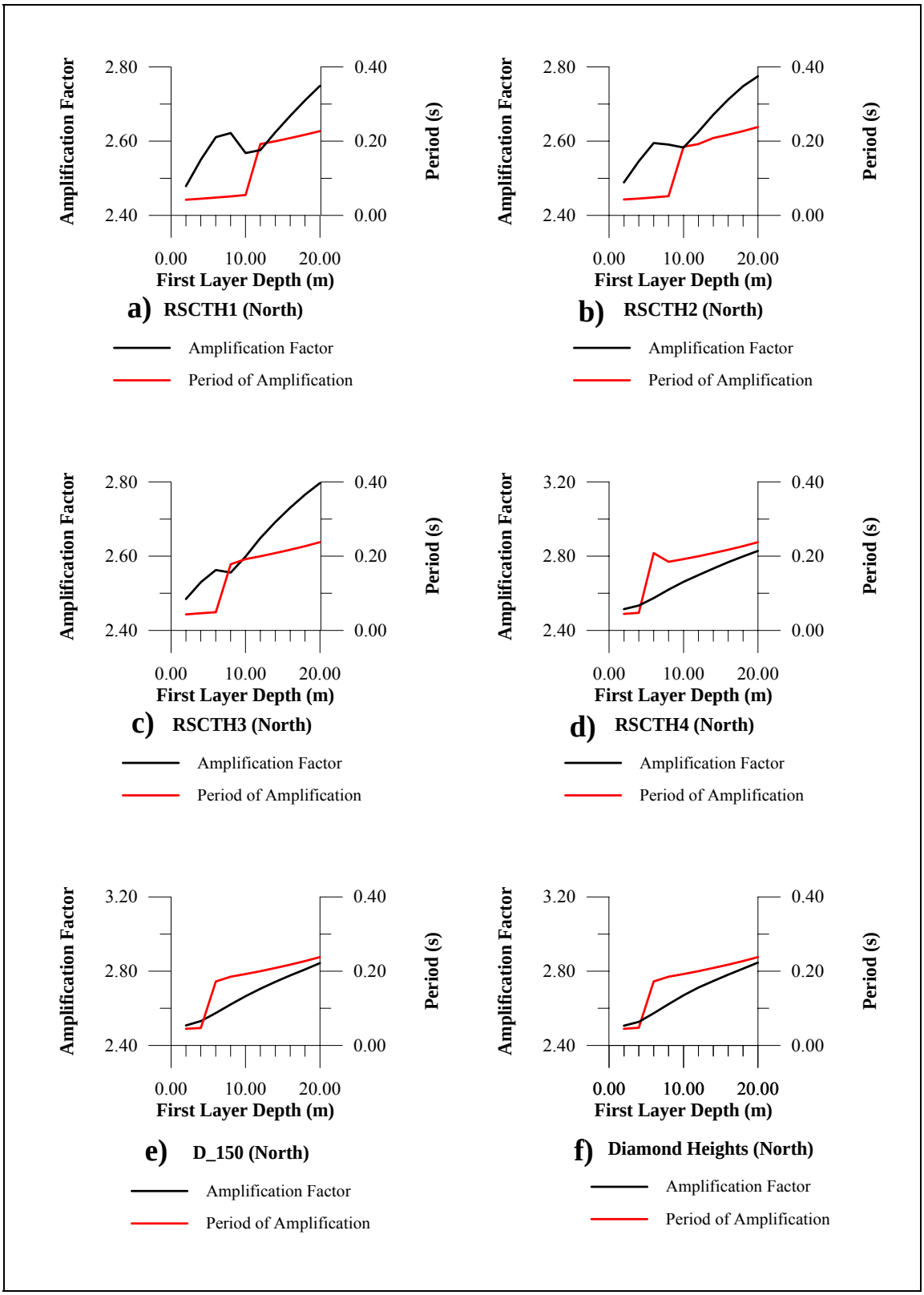

Figure 5.14: Site Response Analysis results for Northerly Albarregas River Soils.

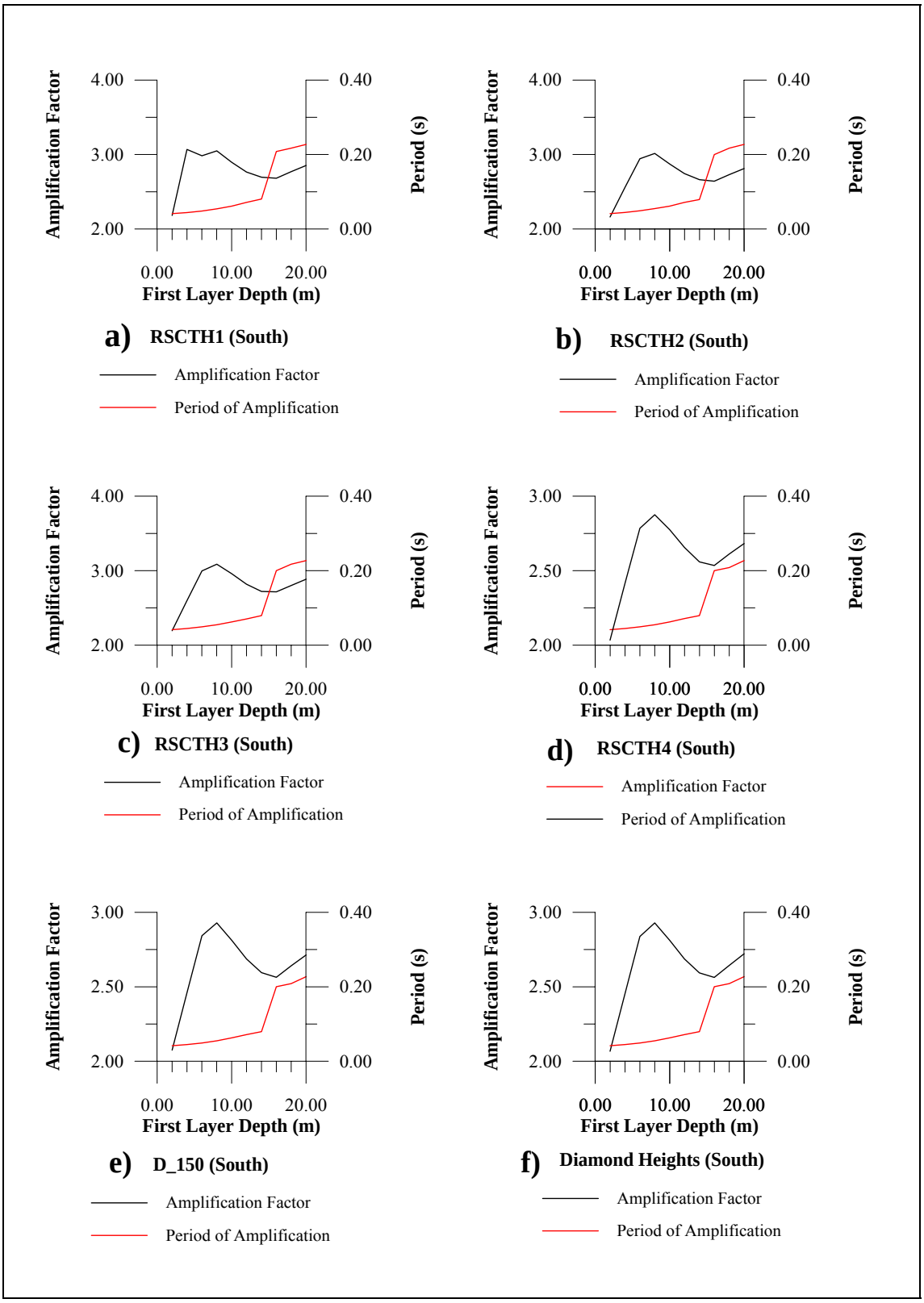

Figure 5.15: Site Response Analysis results for Southerly Albarregas River Soils.

- Surface Response Spectra: as in Northern Albarregas River soils, average surface response spectra through all thicknesses considered has been estimated. Results concerning the periods of maximum amplification in response spectra are similar to those in the previous soil type. Maximum value in the Average Surface Response Spectra

is about 0.57g at Period 0.21 s. Values greater than 0.30 g in acceleration are located between Periods 0.08 and 0.82 s (see Figure 5.16 c).

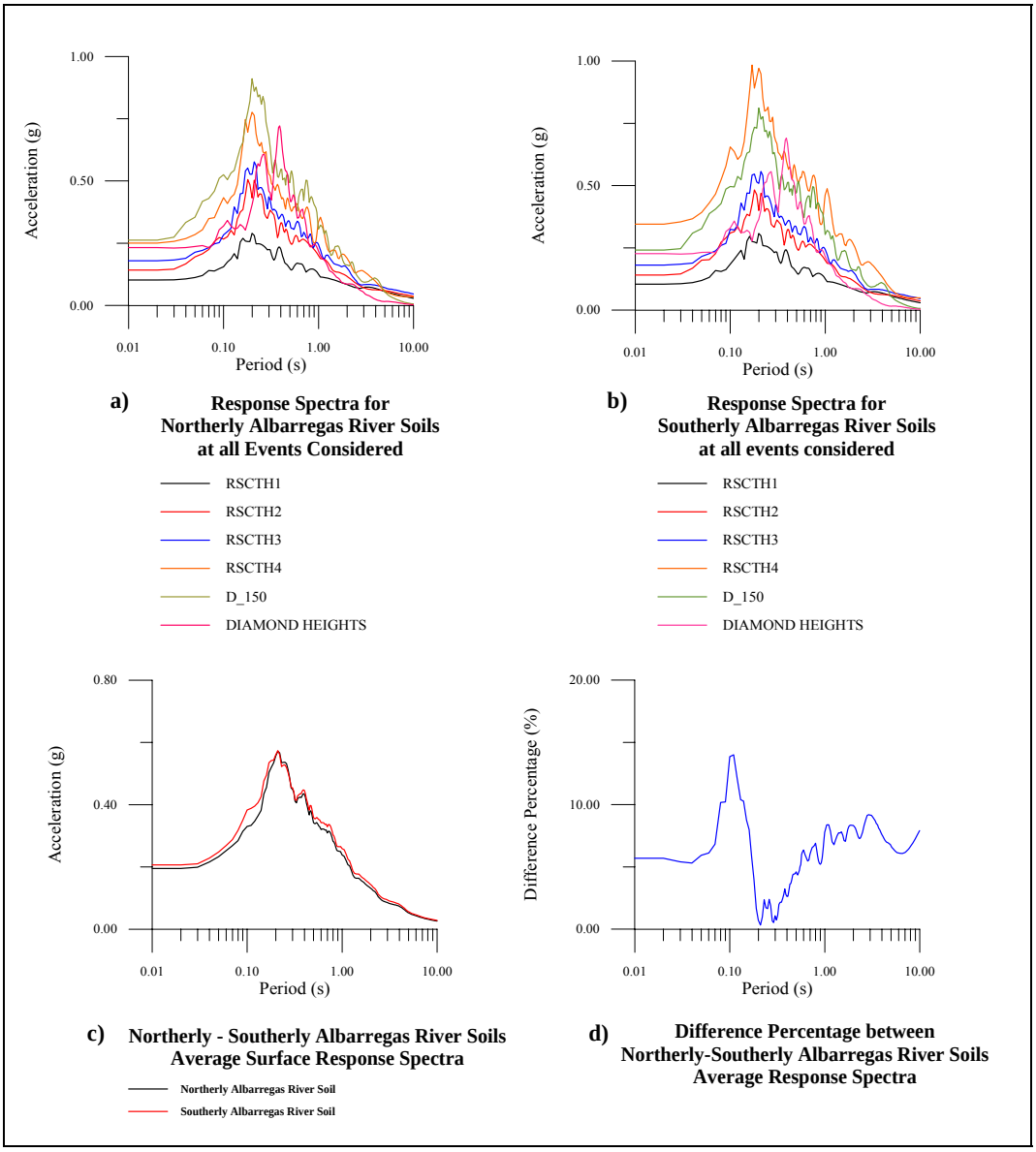

Figure 5.16: Northerly – Southerly Albarregas River Soils Surface Response Spectra.

The difference between the average response spectra for the soils at northerly and southerly Albarregas River (Figure 5.16 c), show a slight difference in acceleration values, greater for the southerly Albarregas River soils, and ranging from around a 5% between 0.01 and 0.05 s Periods, and having a maximum of 15% around 0.10 s Period.

Other authors, such as [Montilla, 1998] and [Hernandez and De Barcia, 1998] have treated the surface response issue in Mérida's Tableau through ambient vibration and small seismic events analyses.

In [Montilla, 1998], Nakamura methodology is performed for a series of 3 hours time-spaced records (gathering 24 hours of monitoring) for ambient vibrations in two different days with different cultural noises (quiet-day and noisy-day), also, the same methodology is applied to

small seismic event records, all analysis in location STN5 (see Map 5.3). The monitoring sites correspond to deep alluvial deposits at the southerly edge of the Tableau. Conclusions are that the response is stationary to cultural noise, variations in the fundamental frequency of the deposit (comparing quiet-day to noisy-day) are small and values are around 4.0 and 5.0 Hz (Average Period: $T \cong 0.22\,s$), amplification factors are around values 2 and 2.5 in the transfer function. These conclusions show a reasonably good agreement with the results obtained in this research, as maximum amplifications periods obtained in deeper soils (16.0 to 20.0 m thickness of first layer) for Southerly Albarregas River Soils, are around Periods $0.20\,s \le T \le 0.23\,s$ and Amplification Factors ranging from 2.6 to 2.9 times the input in all events considered (see Figure 5.15).

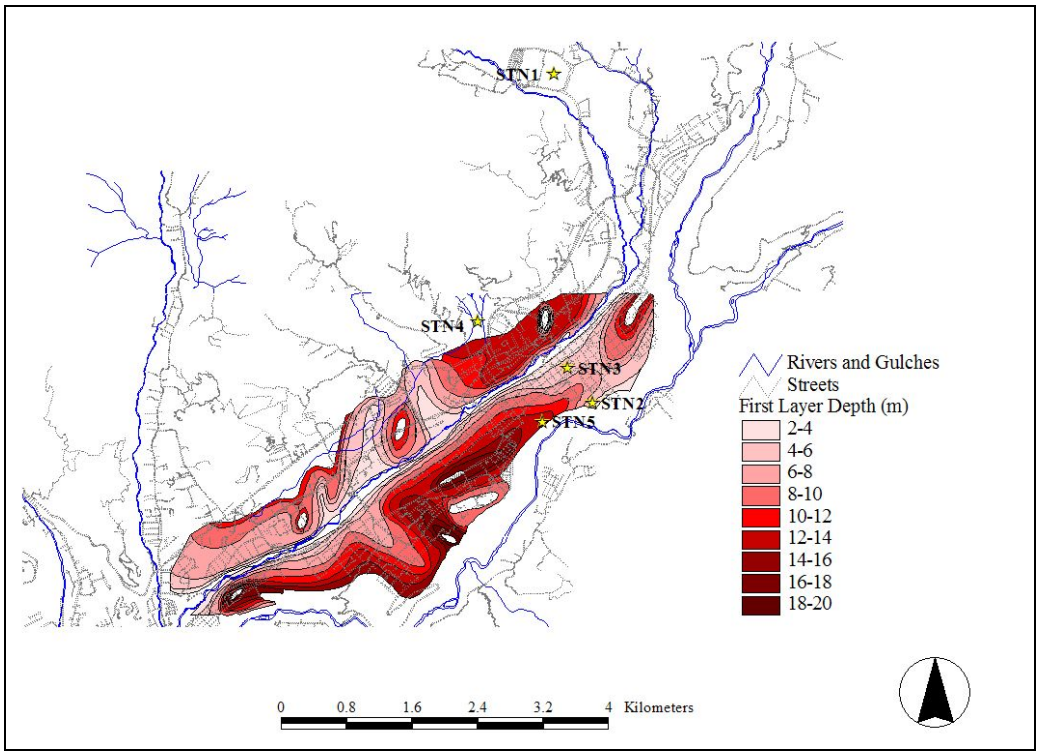

Map 5.3: First Layer Depth Data Available and Ambient Vibration Stations in [Montilla, 1998] and [Hernandez and De Barcia, 1998].

Authors [Hernandez and De Barcia, 1998], perform a similar procedure with Nakamura methodology applied to ambient vibrations at different locations in Mérida's tableau, identified in Map 5.3 as STN1, STN2, STN3, and STN4; and for small seismic events recorded at STN5.

The aforementioned research concludes that in STN1 and STN2 fundamental or predominant frequencies range from 2 to 3 Hz (0.5 s to 0.33 s Periods), while in STN3 values for frequencies range from 3 to 4 Hz (0.33 s to 0.25 s Periods); and at north, where the contact zone appears in mountain foothills northerly Albarregas River (STN4), softer soils have predominant frequencies ranging from 0.3 to 0.6 Hz. The amplifications are related to the depth of sediments where no great differences are observed between the different types of soils. Similarities with this research arise in the considerations of fundamental frequencies for the deposits obtained (STN2 and STN3); the other locations are out of the scope for data available in the present research (STN1 and STN4 in Map 5.3).

5.4.3.2 Mapping and analyzing the seismic hazard scenarios

Data visualization and mapping is nowadays a very powerful tool for decision making processes, the assessments performed in a region or an urban zone must have a graphic expression so to facilitate data comprehension and the consequent decisions to be taken by specialists, researchers and administrators. Geographical Information Systems (GIS) are data visualization tools that allow the analysis of complicated data sets in a dynamic manner.

Throughout this research, all results from analyses are introduced as datasets in a selected GIS so to produce the necessary graphic expression for the comprehension of all data exposed, and an ulterior decision-making process. The tool selected for visualization is the ArcView® GIS software, the reason for choosing this specific software lies in the opportunity to adequate this data for the use of an Earthquake Loss Estimation Methodology such as, for instance, HAZUS®99 [HAZUS-99-SR2, 2002].

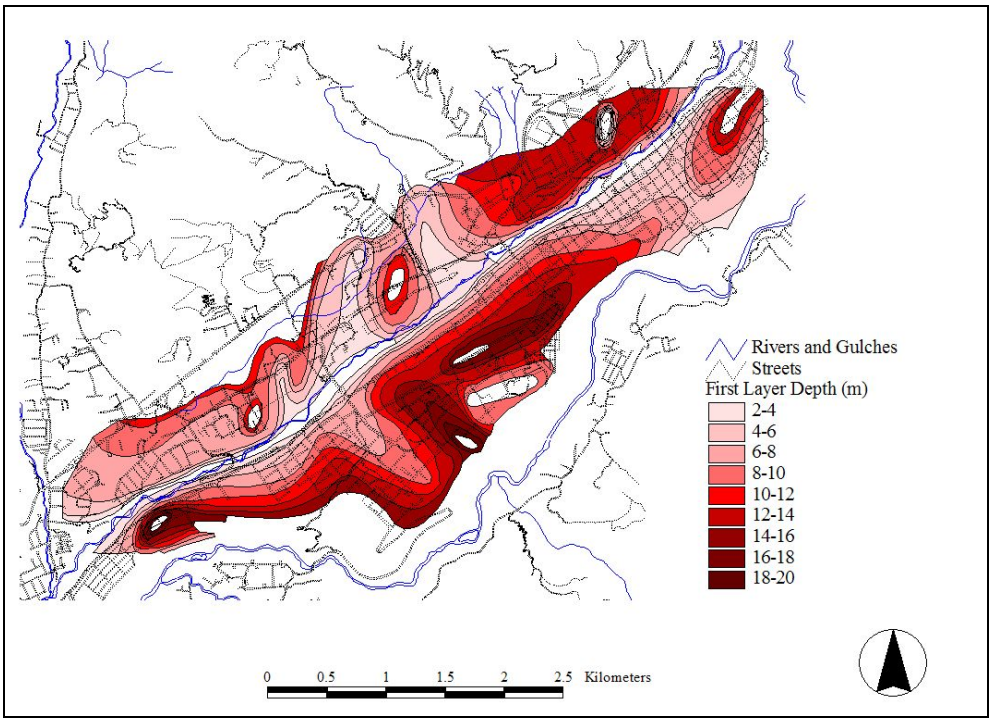

Map 5.4: First Layer thickness for soils in Mérida data from [MOP, 1976].

Based in the results described in the previous section, Site Response Maps are produced showing First Layer Thickness intervals and expected maximum amplification factors and periods of maximum amplifications at each thickness interval, for the scenario events considered, at each soil type at North and South of the Albarregas River. The Amplification Factors and the Periods of Maximum Amplification, for the maps, are obtained through an average of these values estimated for the different acceleration records (six in total) at each of the first layer thickness intervals (ten in total), for the two typical soil columns in Mérida's tableau.

Amplification Factors and Periods of Maximum Amplification

The following maps represent, by separate, the different results obtained in this section of the research. In Map 5.4, the thickness of the First Layer is shown; it may be appreciated how deeper soils are mostly located at the southern flank of the tableau at the limits of the Chama River canyon (up to 150 m deep). First Layer thickness information for the map is that available in [MOP, 1976], information covers the tableau in its geomorphologic limits, this due to the size of the city at the time of the study (years 1973-74).

Amplification Factors (AF) for the scenario event *I* = VI are shown in Map 5.5. It may be seen how soils located southerly Albarregas River respond with relatively higher AF's than the northerly soils. The same may be observed in Figure 5.14 and Figure 5.15, where site response is plotted for Amplification Factors and Periods of Maximum Amplification versus First Layer thickness.

For scenario event *I* = IX (Map 5.6), the ranges in AF's are relatively close to those in scenario event *I* = VI, and for both it may be noted that at southerly Albarregas River soils surface layer thicknesses between 4.0 m and 8.0 m present the highest amplification factors, around a 10% higher than northerly soils with identical first layer thickness (see also Figure 5.16 c).

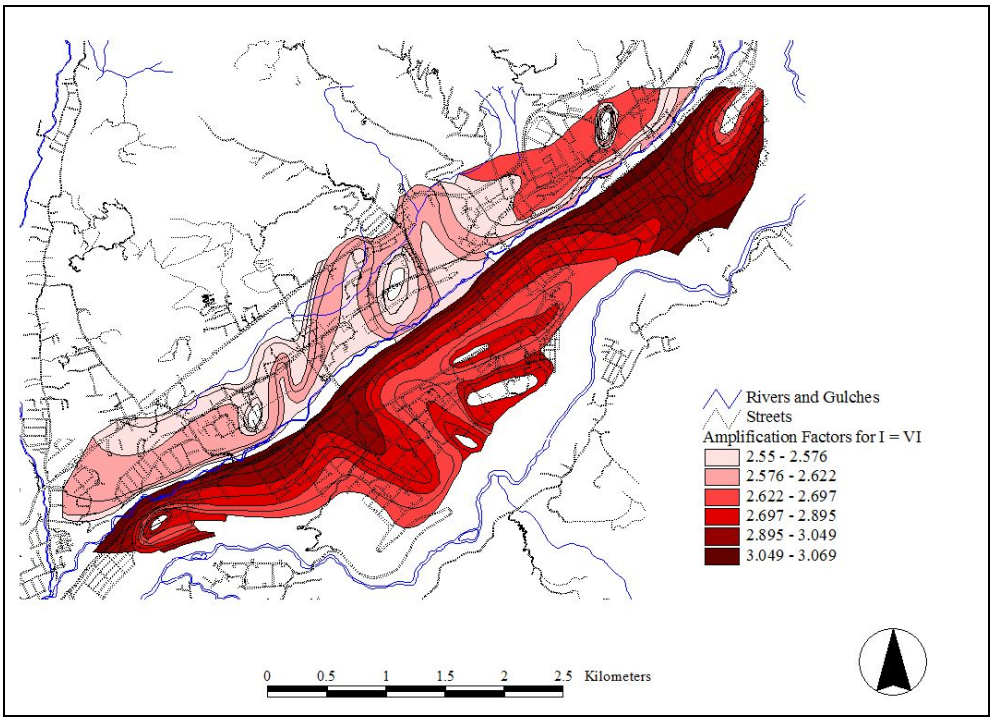

Map 5.5: Amplification Factors for Scenario Event *I* = VI.

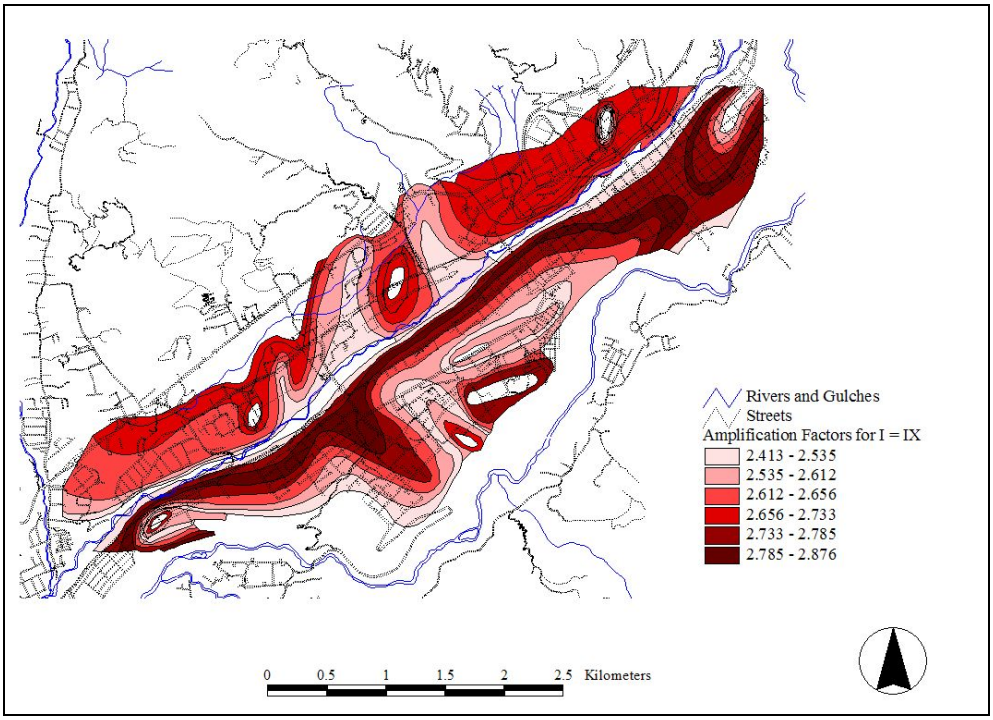

Map 5.6: Amplification Factors for Scenario Event *I* = IX.

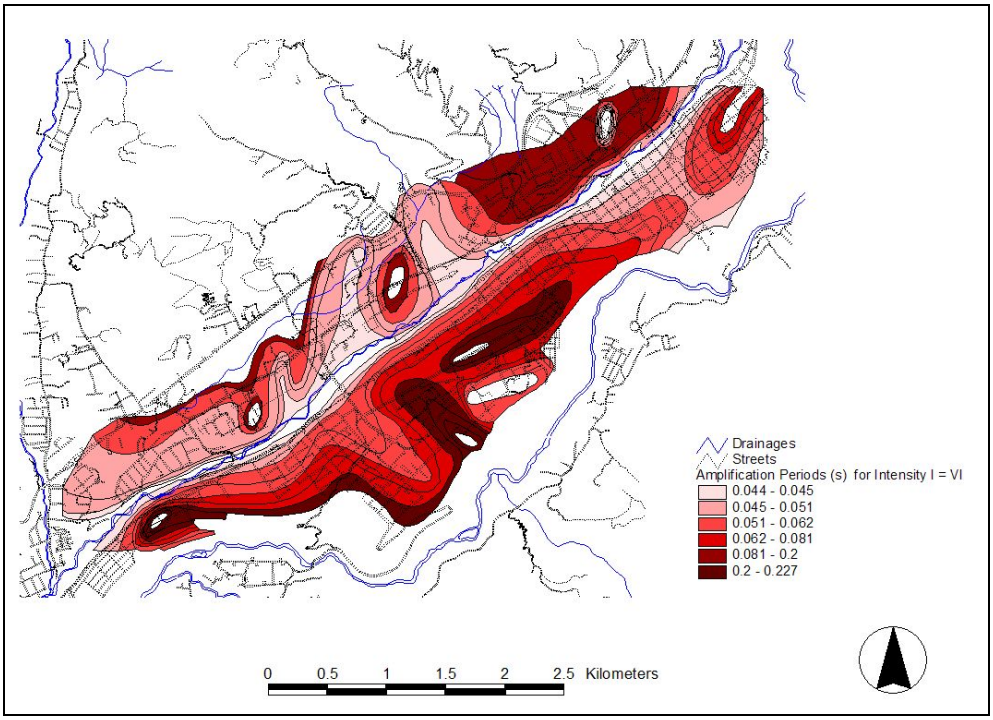

Map 5.7: Periods of Maximum Amplification for Intensity *I* = VI Event.

Lower and upper boundaries for AF'S values for all events considered at either sides of the Albarregas River, are 2.416 and 3.069 times the input, respectively. It may be stated that for Mérida's Tableau, amplifications are in the range of 2.5 to 3 times the acceleration input.

Taking into account the Amplification Factors at different thicknesses of the first layer, it is possible to estimate the seismic amplification as a local increment of the macroseismic intensity degree. Goretti and Dolce (2004), state that the seismic amplification expressed in terms of ground motion parameters (as for example, the PGA), may also be expressed in terms of an increment in the macroseismic intensity, by means of a conversion law that has the form:

$$F_a = \frac{Y}{Y_{REF}} = 10^{0.22(I - I_{REF})} = 10^{0.22\Delta I} \qquad \text{eq. 5.7}$$

Where Y and Y_{REF} are, the amplified ground motion parameter and the reference ground motion parameter of the event, respectively; and $\Delta I = I - I_{REF}$ is the increment of the macroseismic intensity.

To perform such conversion, the average amplification factors at each first layer thickness for the events considered is estimated, the reference ground motion parameter (Y_{REF}), which in this case is the PGA, is taken as the lowest value of amplification obtained for a first layer thickness. Operating with the different values of AF's at the different first layer thicknesses the values of the increment in macroseismic intensity may be estimated by equation 4.7 written as:

$$\Delta I = \frac{\log(F_a)}{0.22} \qquad \text{eq. 5.8}$$

The increments in the macroseismic intensity degree are sought as the values of ΔI between 0.5 and 0.7 and are considered as middle intensity degree values in the scale. From the results, the southerly Albarregas River soils with first layer thicknesses ranging from 4.0 m to 10.0 m, and with first layer thickness from 18.0 m to 20.0 m, are found with amplifications that converted correspond to upper middle values of the intensity degree. On the other hand, for the soils at northerly Albarregas River the amplifications do not correspond to middle values of intensity degree in the conversion. In this fashion, the soils with middle values of intensity degree for each of the intensities considered are shown in Map 5.8, which correspond with the maximum amplification factors (upper ranges of AF's) in the I = VI and I = IX Amplification Factors shown in Map 5.5 and in Map 5.6.

Periods of Maximum Amplification (PMA) for the first scenario earthquake considered (see Table 5.8) are shown in Map 5.7. In the data mapping, it is verified how deeper soils generate larger periods of site response. It shows how a slight difference arises in resulting period values for an identical first layer thickness at both sides of the Albarregas River. Local site conditions account for these differences, as soil compositions are different at one and other side of the river (Table 5.9).

In order to obtain additional information about the following events considered in the analysis, normalization via the first event (EMS Intensity I = VI) results for Periods of Maximum Amplification (PMA), is performed over the other events PMA'S, i.e. a normalization equation that has the form:

$$N_{PMA\left(\frac{VII}{VI}\right)} = \frac{PMA(VII)}{PMA(VI)}, \qquad \text{eq. 5.9}$$

Where:

PMA(VII) is the PMA for every First Layer Thickness Interval for an event: I = VII.

PMA(VI) is the PMA for every First Layer Thickness Interval for the first event: I = VI.

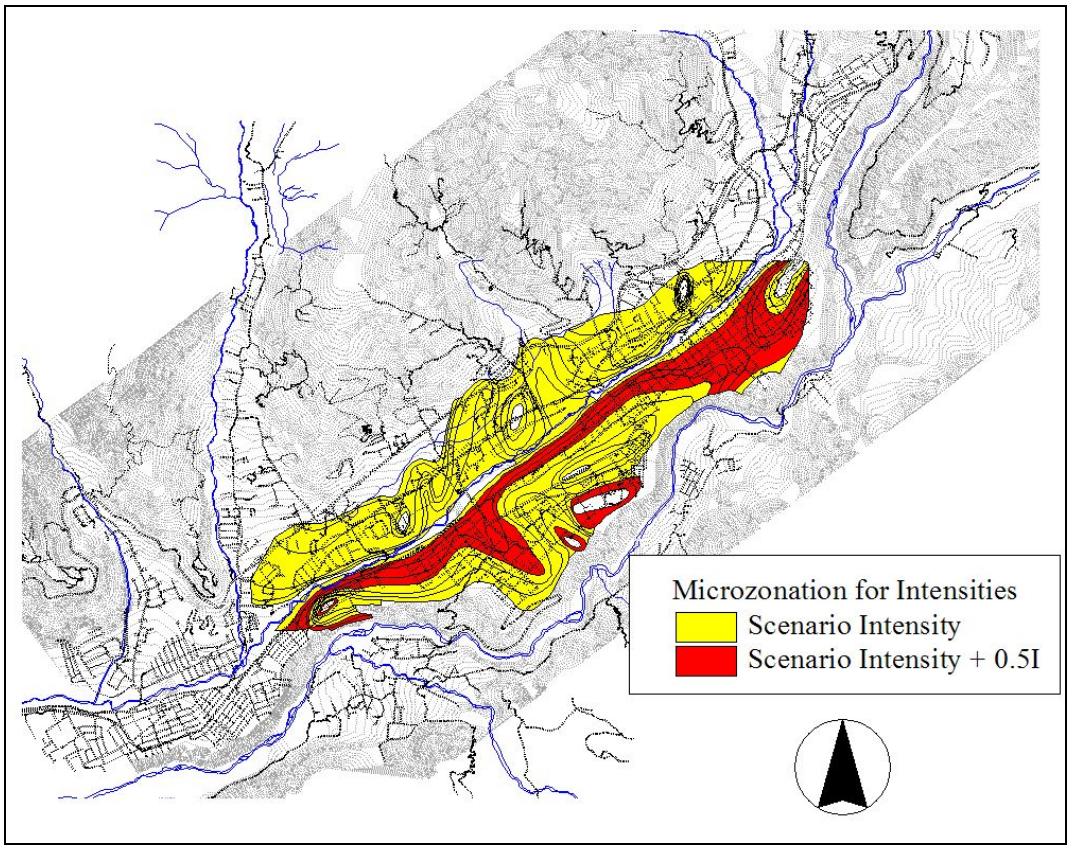

Map 5.8: Increments of intensity degree for the soils in the tableau.

Through this approach, changes in PMA'S produced by an increment in earthquake magnitude for the successive scenario events may be mapped and presented as visualized data in a GIS. As an Example, in Map 5.9, normalized PMA'S for the event Intensity *I = IX* is shown. It may be verified how most of the soil remain between values 0.96 and 1.52 times the Periods for the first event, and at north of the Albarregas River, at First Layer Depth intervals from 4.0 to 10.0 m the periods increase between 3.77 to 4.33 times.

The reliability of the results depend essentially on the quality of information available and the methodology used in the analysis, for the case of this research results are confirmed at some extent by crossing with other investigations using a different approach, such as Micro tremor and ambient vibration records analysis through Nakamura methodology cited previously. The One-Dimensional Equivalent Linear Site Response approach, *"… based on the assumption that all boundaries are horizontal and that the response of a soil deposit is predominantly caused by SH-waves propagating vertically from the underlying bedrock …"* [Kramer, 1996], may prove incapable of detecting fundamental frequencies and amplification factors at locations with topographic irregularities. In Mérida's case, locations near deep canyons, ridges, or in alluvial basins with specific complex geometry, may generate unexpected significant effects on ground motion. In addition, it is probable that linearity in equivalent linear approach may generate spurious resonances from the *"… coincidence of a strong component of the input motion with one of the natural frequencies of the equivalent linear soil deposit …* " [Kramer, 1996].

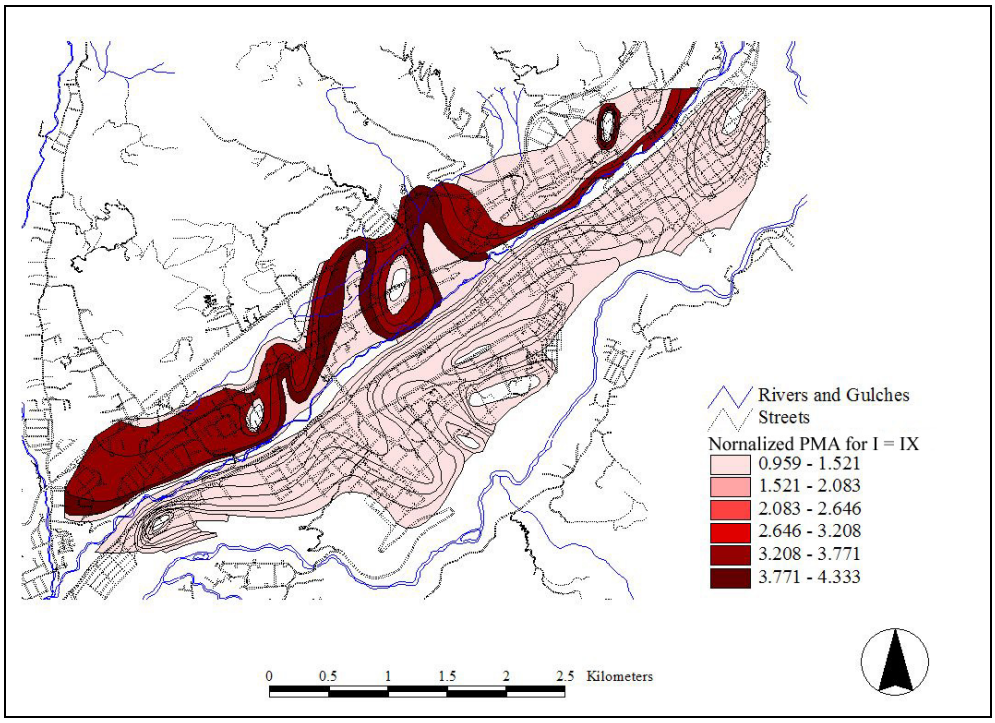

Map 5.9: Normalized Periods of Maximum Amplification for Intensity *I* = IX event.

5.4.4 Earthquake Induced Effects

Ground shaking is the fundamental cause of damage and losses in an earthquake, as it may induce different effects at different sites in an interest zone. The most damaging effects correspond to those phenomena related to permanent ground displacements, in which the geometry of the site may suffer changes affecting adversely the constructions and facilities built upon it. Through experience with past earthquakes, (the 1964 Good Friday earthquake in Alaska, USA, the 1964 Niigata-Japan earthquake, the 1999 El Quindío-Colombia earthquake, and others) two permanent ground displacements-related phenomena have risen as the most damage generators: Soil Liquefaction and Earthquake-Induced Landsliding.

Soil Liquefaction phenomena is related to rapid cyclic loading in cohesionless undrained soils, which tends to soil densification generating increasing excess pore pressures and decreasing effective stresses in the soil. Two main phenomena groups describe different liquefaction effects: flow liquefaction and cyclic mobility [Kramer, 1996].

- Flow liquefaction occurs when the static shear stress required for static equilibrium is greater than the shear strength of a liquefied soil; static shear stresses then drive the deformations generated by flow liquefaction. Displacements generated by flow liquefaction may be in the order of meters to tens of meters (flow slides) with possible catastrophic consequences in surrounding areas.
- Cyclic mobility occurs when the static shear stress is lower than the shear strength of a liquefied soil; both the static and cyclic shear stresses drive the deformation. Displacements and consequent deformations may be different in nature depending on the geometrical character of the site:
    - Lateral spreading, which may occur in gentle slopes or in flat ground adjacent to bodies of water, static horizontal shear stresses drive deformation and displacements may be in the order of centimeters or a few meters with the appearance of surface fissures and slumping.

- Level-ground liquefaction may occur in flat terrain susceptible to liquefaction. As static horizontal shear stresses are not present, it may produce large vertical ground oscillation movements with little permanent lateral soil deformations. Failure is produced by an upward flow of water generated when seismically induced excess pore pressures dissipate generating vertical settlements. Excessive vertical settlements with consequent low-lying land flooding and the appearance of sand boils are characteristic of this liquefaction phenomenon.

Earthquake-Induced Landsliding relates to the failure of slopes that were marginally to moderately stable before the earthquake, this type of phenomenon has generated large amounts of damage through history, being able to reach catastrophic consequences accounting for more damage than all other seismic hazards combined. The slope's geometry and material characteristics determine the resulting displacements, which may generate damage ranging from insignificant to catastrophic.

As complexity and uncertainties arise in the study of these two ground motion-induced phenomena, where each have different factors and characterizations, susceptibility concept is used to detect whether a certain site is sensible or not to suffer such deformations, under categorizations such as Very High, High, Moderate, Low and Very Low susceptibilities. For the screening of possible occurrence of these potential hazards, susceptibility has to be assessed, and if it exists, at which ground motion parameter values is triggered, and if triggered, what amount and kind of damage-generating displacements may occur.

Various methodologies are available to perform potential hazard assessments for liquefaction and earthquake-induced landslides. In this research, the approach used is that of HAZUS®99 Earthquake Loss Estimation Methodology. The choice of this specific methodology relies in the fact that has been successfully used throughout the USA, with the GIS tool ArcView® as the data visualization platform. Assessments are then performed in the fashion of HAZUS®99 methodology, for which a summary explanation is presented.

HAZUS®99 Earthquake Loss Estimation Methodology: the Federal Emergency Management Agency (FEMA) in cooperative agreement with the National Institute of Building Sciences has developed HAZUS® methodology. This methodology stands for "Hazard USA", responding to the objective of mitigation as means of reducing damages and social-economic impacts from earthquakes in the United States of America. As a prediction tool for a wide range of different types of losses, provides local, state, and regional officials with a decision-making support to estimate future losses from scenario earthquakes and anticipating its consequences, assisting the development of plans and strategies for risk reduction.

The visualization platform is a GIS-based software that may be used at multiple resolution levels for different levels of user expertise, it is divided in different modules addressing various user requirements providing additional flexibility in a diversity of applications. Assessment is performed through built-in data corresponding to the area of interest comprising information on ground response (Amplification Factors, Periods of Maximum Amplification, and the probability of occurrence of several induced effects – landsliding, liquefaction- and their expression as Permanent Ground Displacements) for diverse scenario events, denominated Potential Earth Science Hazards. Facilities and buildings are considered using vulnerability indexations, and the probable damaging effects distribution and its cost generated by the scenario events. Scenarios may show not only damage distribution over a specific area, but also the casualties, wounded and the economic impact in the area (by means of population and economic built-in data - from census tracts -). Although limitations arise in the sense of overestimations in ground response (where specific data is still not available, conservative approach is performed), and modeling of vulnerabilities (incomplete scientific knowledge concerning earthquakes and their effect upon buildings and facilities), the

methodology is understood as a work in progress in which through experiences permanent calibrations are possible.

As built-in data is not available for regions outside the USA, the several inputs needed for assessments are built in a GIS tool (ArcView®) with the data available for this research case, the city of Mérida in Venezuela. Evaluation for liquefaction and landsliding potential through HAZUS®99 methodology is explained in the following, with adequate data inclusion to cover the interest zone for this research.

5.4.4.1 Liquefaction Susceptibility Assessment.

For Liquefaction Susceptibility, two maps are necessary, the geologic and the Geomorphologic maps. Based in maps from the Venezuelan Ministry of Mines and Oil [Ministerio de Minas e Hidrocarburos, 1974], corresponding Geologic and Geomorphologic data are included into a Geographical Information System (ArcView®) database. Treatment for data is based in HAZUS® methodology for Potential Earth Science Hazards -PESH- [HAZUS-99-SR2, 2002].

Liquefaction susceptibility: liquefaction hazard evaluation implies the characterization of the relative liquefaction susceptibility of the soil by means of the geologic conditions of a region or sub-region. In [Youd and Perkins, 1978], a classification system for liquefaction susceptibility is proposed related to geologic age and type of sedimentary deposits, establishing the likelihood that cohesionless sediments distributed in deposits (when saturated) would be susceptible to liquefaction, five levels of susceptibility are proposed: Very High, High, Moderate, Low and Very Low (see Table 5.11).

In Map 5.10, Geologic Age of Deposits distribution is shown for the Tableau of Mérida, older deposits (Holocene geologic era) are at the northerly and southerly mountain foothills limits of the tableau, the city is sited in the younger deposits (Pleistocene geologic era). In Map 5.11, the Geomorphology of Deposits is shown; most of the city is sited over an Alluvial Plain, originally the richest soils for agricultural activities, and site of the foundation. The growth of the city in the second half of the 20th century forced the use of surrounding lands with other geomorphologies, such as the Colluvium and Alluvial Fan zones.

Liquefaction susceptibility for deposits in Mérida is Low in most of the tableau's surface (Map 5.12); only for colluvial deposits a Moderate susceptibility is observed. However susceptibility is detected, the triggering ground motion parameter values have to be determined, and verify if local site ground response parameter values are in the triggering threshold for liquefaction to occur.

Type of Deposit	General Distribution of Cohesionless Sediments in Deposits	Likelihood that Cohesionless Sediments when saturated would be susceptible to Liquefaction (by age of deposit)			
		< 500 years Modern	Holocene < 11 ka	Pleistocene 11 ka – 2 Ma	Pre-Pleistocene > 2 Ma
(a) Continental Deposits					
River Channel	Locally Variable	Very High	High	Low	Very Low
Flood Plain	Locally Variable	High	Moderate	Low	Very Low
Alluvial Fan and Plain	Widespread	Moderate	Low	Low	Very Low
Marine Terraces and Plains	Widespread	----	Low	Very Low	Very Low
Delta and fan-delta	Widespread	High	Moderate	Low	Very Low
Lacustrine and Playa	Variable	High	Moderate	Low	Very Low
Colluvium	Variable	High	Moderate	Low	Very Low
Talus	Widespread	Low	Low	Very Low	Very Low
Dunes	Widespread	High	Moderate	Low	Very Low
Loess	Variable	High	High	High	Unknown
Glacial Till	Variable	Low	Low	Very Low	Very Low
Tuff	Rare	Low	Low	Very Low	Very Low
Tephra	Widespread	High	High	Unknown	Unknown
Residual Soils	Rare	Low	Low	Very Low	Very Low
Sebka	Locally Variable	High	Moderate	Low	Very Low
(b) Coastal Zone					
Delta	Widespread	Very High	High	Low	Very Low
Esturine	Locally Variable	High	Moderate	Low	Very Low
Beach High Wave Energy	Widespread	Moderate	Low	Very Low	Very Low
Low Wave Energy	Widespread	High	Moderate	Low	Very Low
Lagoonal	Locally Variable	High	Moderate	Low	Very Low
Fore Shore	Locally Variable	High	Moderate	Low	Very Low
© Artificial					
Uncompacted Fill	Variable	Very High	----	----	----
Compacted Fill	Variable	Low	----	----	----

Table 5.11: Liquefaction Susceptibility for Sedimentary Deposits [Youd and Perkins, 1978].

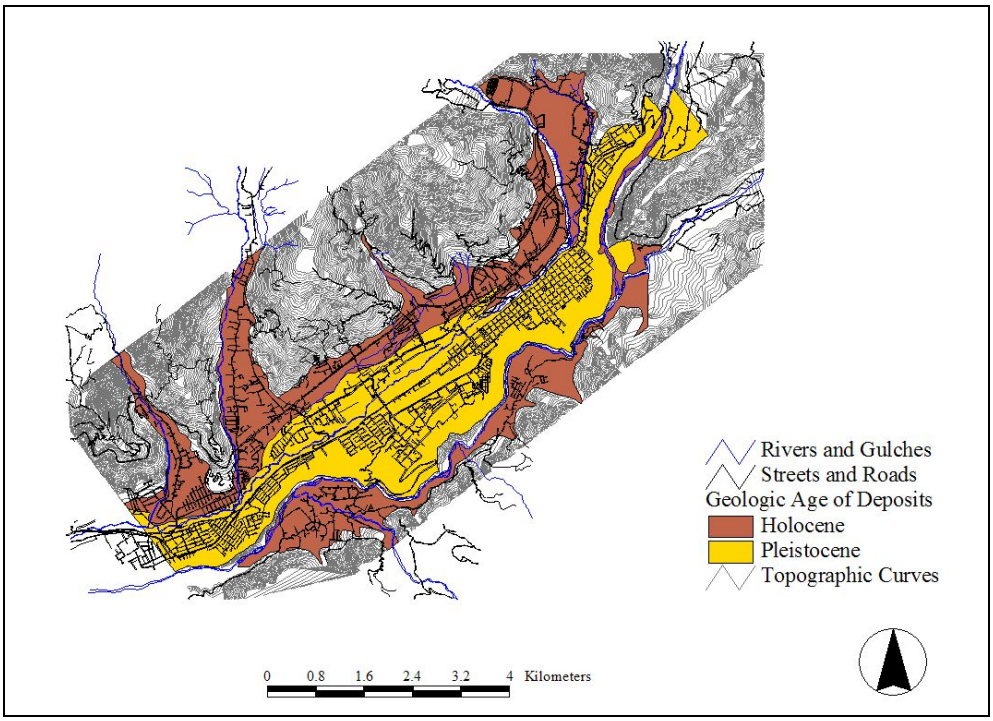

Map 5.10: Geologic Age of Deposits for Mérida's Tableau [Ministerio de Minas e Hidrocarburos, 1974].

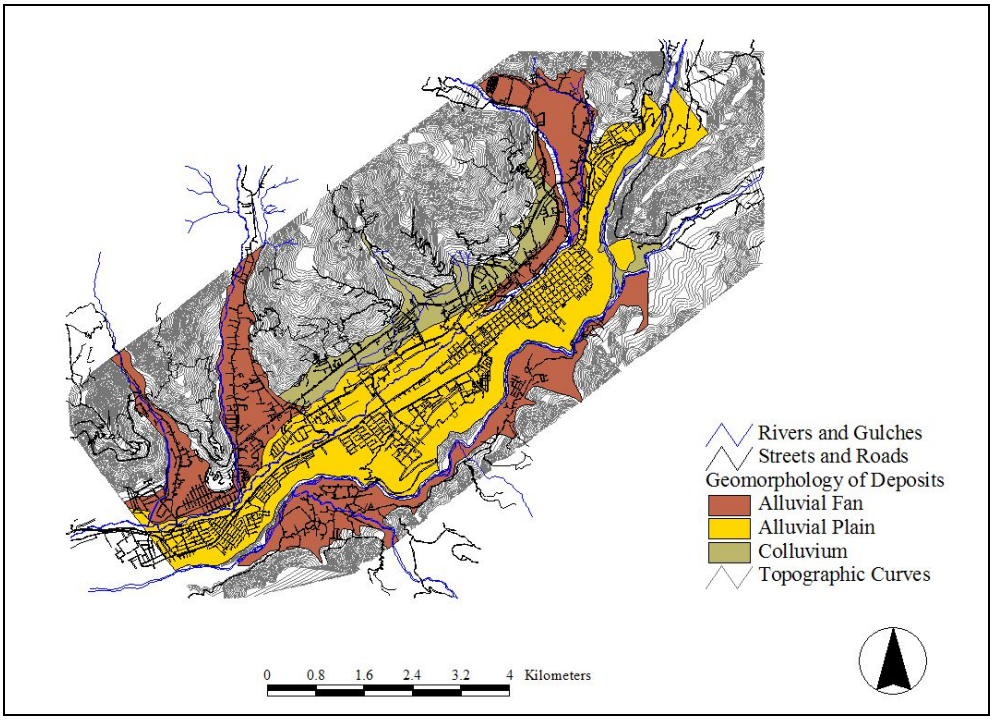

Map 5.11: Geomorphology of Deposits in Mérida [Ministerio de Minas e Hidrocarburos, 1974].

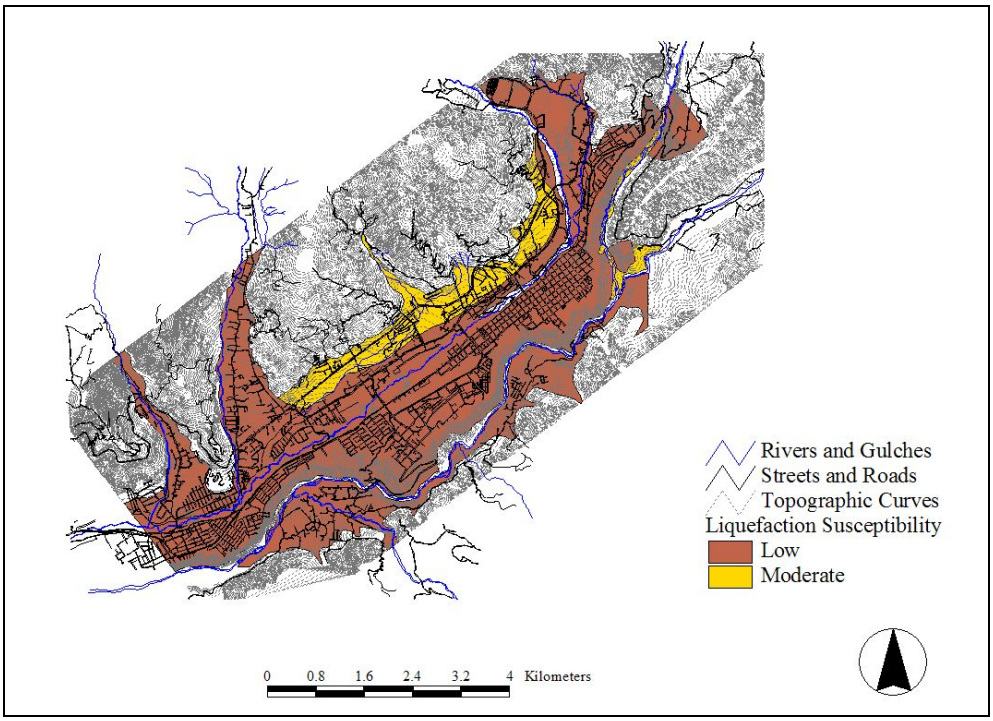

Map 5.12: Liquefaction Susceptibility for Soil Deposits in Mérida's Tableau.

Liquefaction Probability:

Likelihood of liquefaction in soils is primarily influenced by the susceptibility of the soil, the amplitude (PGA) and duration (Magnitude) of ground shaking and water table depth. In addition, because natural geologic deposits as well as man-made fills encompass a range of liquefaction susceptibilities (due to variations of soil type, relative density, soil's grain distribution, etc.), portions of a geologic map unit may not be susceptible to liquefaction, expecting non-susceptible portions to be smaller for higher susceptibilities. In the HAZUS® methodology [HAZUS-99-SR2, 2002], this fact is considered by means of a probability factor that quantifies the proportion of a geologic map unit susceptible to liquefaction related to the susceptibility classes. In Table 5.12, suggested default values in methodology for these proportions are shown.

General form for the probability of liquefaction given a susceptibility class is:

$$P\left[liquefaction_{SC}\right] = \frac{P\left[liquefaction_{SC} \middle| PGA = a\right]}{K_M K_W} P_{ml} \qquad \text{eq. 5.10}$$

Where: $P\left[\text{liquefaction}_{SC} \middle| PGA = a\right]$, is the conditional liquefaction probability for a given susceptibility class at a specified level *a* of Peak Ground Acceleration *PGA*; K_M ,is the moment magnitude (M) correction factor; K_W is the water table correction factor, P_{ml} , is the proportion of map unit susceptible to liquefaction.

Mapped Relative Susceptibility	Proportion of Map Unit
Very High	0.25
High	0.20
Moderate	0.10
Low	0.05
Very Low	0.02
None	0.00

Table 5.12: Proportion of Map Unit Susceptible to liquefaction, [HAZUS-99-SR2, 2002].

The conditional liquefaction probability has been developed for an earthquake $M = 7.5$ magnitude, and an assumed water table depth of 1.5 m (Figure 5.17).

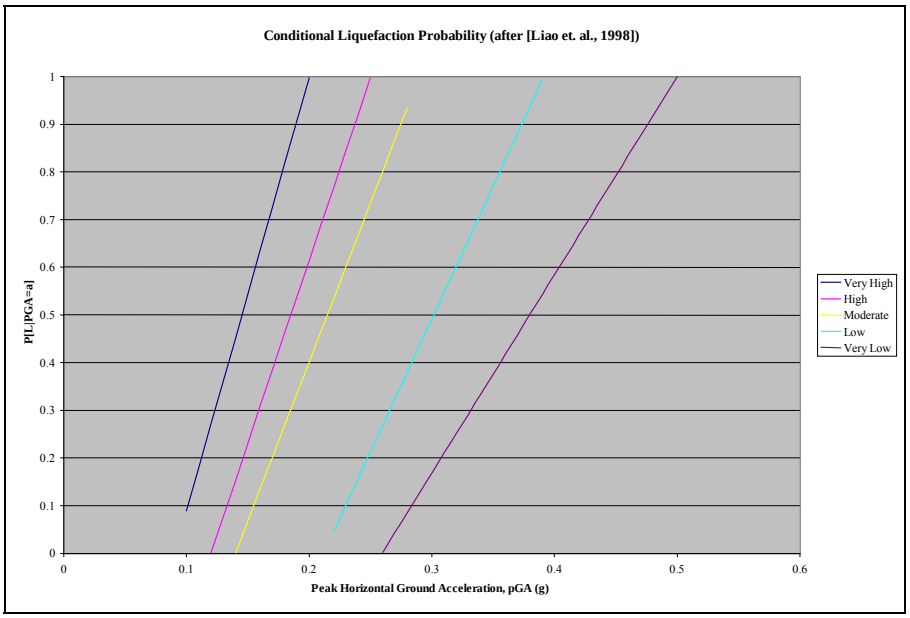

Figure 5.17: Conditional Liquefaction Probability relationships for Liquefaction Susceptibility categories, after [Liao et. al, 1988].

This relationship is defined based in state-of-practice empirical procedures and statistical model for the liquefaction catalog in [Liao et. al., 1988], correction factors for other magnitudes and groundwater depths are also based in empirical state-of-practice procedures to evaluate liquefaction potential [Seed and Idriss, 1982; Seed et. al., 1985; National Research Council, 1985], general forms for relationships are:

$$K_M = 0.0027M^3 - 0.0267M^2 - 0.2055M + 2.9188 \qquad \text{eq. 5.11}$$

Where *M* represents magnitude

$$K_W = 0.022d_W + 0.93 \qquad \text{eq. 5.12}$$

Where d_W represents water table depth.

Probability of liquefaction, $P[\text{liquefaction}_{SC}]$, is calculated for the expected maximum value of magnitude, acceleration level and depth of water table in Mérida's plateau. Based in a set of two maps containing information on Geologic ages and Geomorphology for deposits [Ministerio de Minas e Hidrocarburos, 1974], a database for ArcView®, is built, giving attributes to delimited zones in Mérida city containing specific characteristics pertaining liquefaction susceptibility classes, i.e. geologic age and type of deposit. Each of these zones is treated as a map unit with specific geologic-geomorphologic characteristics incorporating within these the maximum scenario event (resulting from probabilistic seismic hazard analysis).

In Figure 5.18, the Probability of Liquefaction for magnitude M = 6.8 and water table depth 3.0 m (average groundwater depth for the tableau) is plotted based in equations 5.10, 5.11 and 5.12, for the five susceptibility categories. For the case of study, categories for Liquefaction susceptibility are Moderate and Low (see Map 5.12).

Peak Ground Acceleration must be that of the corresponding scenario event multiplied by the amplification factor at the site. In site response analysis results, maximum amplification values are around 3 times the input expecting the worst scenario, then, $PGA_{\max} = 3(0.1646)g = 0.4938g$. For this acceleration, liquefaction probabilities in Moderate and Low categories are 0.02 and 0.007 respectively.

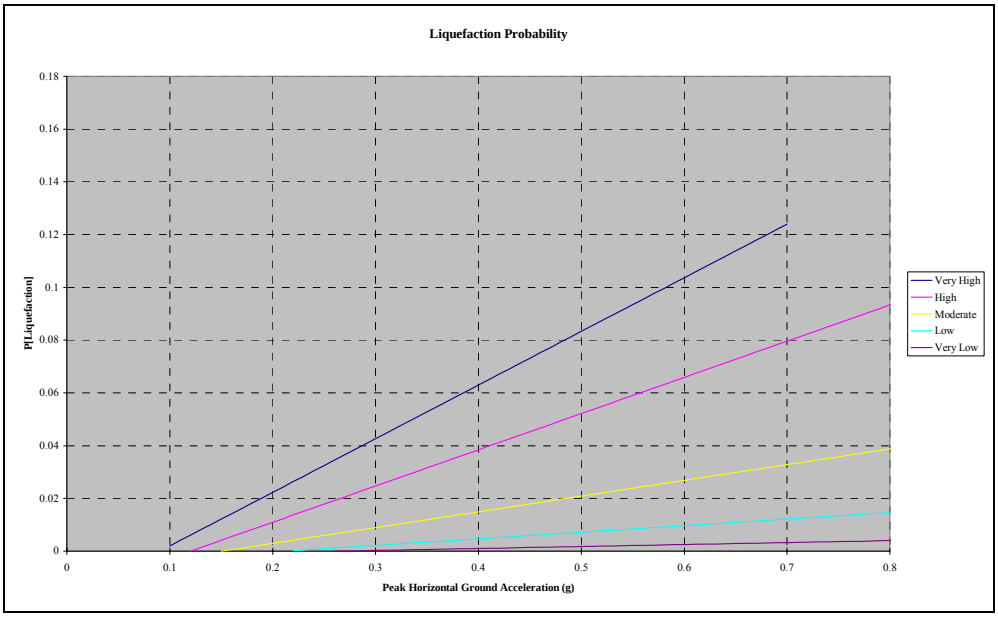

Figure 5.18: Liquefaction Probability for *M* = 6.8 and water table depth of 3.0 m.

Map resulting from Probability of Liquefaction analysis in Mérida's plateau, is shown in Map 5.13. Soils with Low Susceptibility occupy an area of 2,520 Ha, corresponding to an 87.54% of total surface considered; on the other hand, Moderate susceptibility covers 359 Ha, with a 12.46% of soil deposits in the study area.

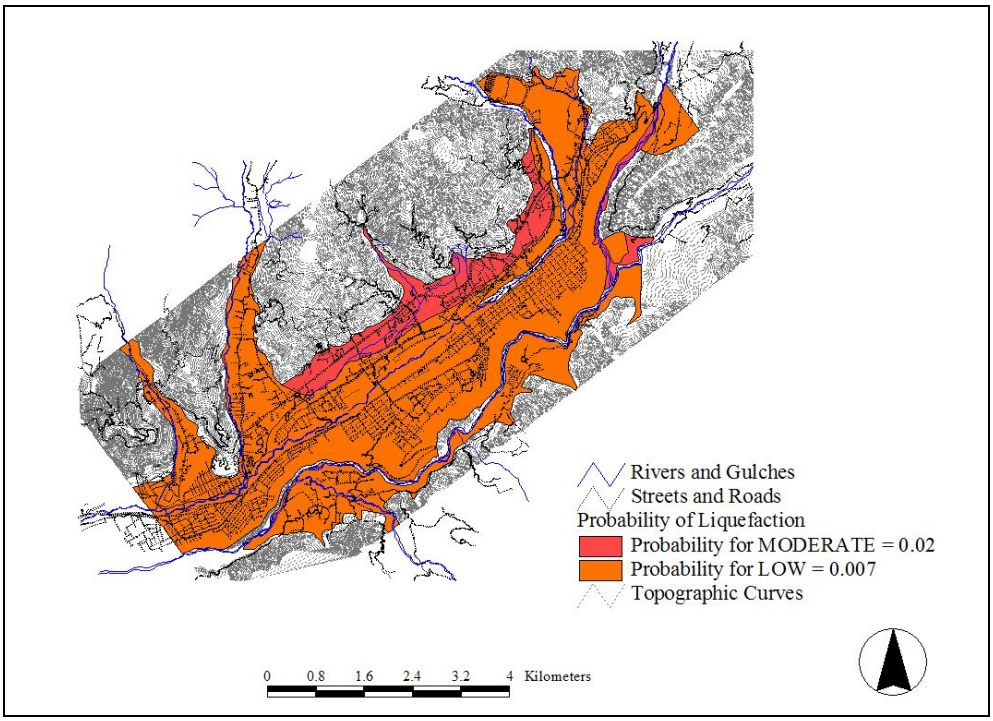

Map 5.13: Liquefaction Probability for *I* = IX Scenario Event.

Permanent Ground Displacements (PGD) estimation for Liquefaction Probability.

Liquefaction assessment through HAZUS® [HAZUS-99-SR2, 2002] methodology considers two types of movements: Ground Settlement and Lateral Spreading, these may generate large deformations when earthquake shaking is acting. Both phenomena are produced when the static shear stress is less than the shear strength of the liquefied soil, where deformations develop incrementally during shaking driven by cyclic and static shear stresses.

For Lateral Spreading, the expected permanent ground displacements are estimated through the relationship:

$$E\left[PDG_{SC}\right] = K_{\Delta} \cdot E\left[PDG \middle| \left(PGA / PL_{SC}\right) = a\right] \qquad \text{eq. 5.13}$$

The displacement term: $E\left[PDG \middle| \left(PGA / PL_{SC}\right) = a\right]$, is the expected permanent ground displacement for a given susceptibility category under a specified level of normalized ground shaking ($PGA/PGA(t)$) shown in Figure 5.19; it is based on earthquakes with magnitude M = 7.5. Displacements for other magnitudes are estimated by a displacement correction factor K_{Δ}, given by equation 5.14. Peak ground acceleration threshold $PGA(t)$, (shown in Table 5.13) is the triggering ground acceleration to induce liquefaction, based in zero probability of Conditional Liquefaction (Figure 5.17) for each susceptibility category.

$$K_{\Delta} = 0.0086M^{3} - 0.0914M^{2} + 0.4698M - 0.9835 \qquad \text{eq. 5.14}$$

Where, M is moment magnitude.

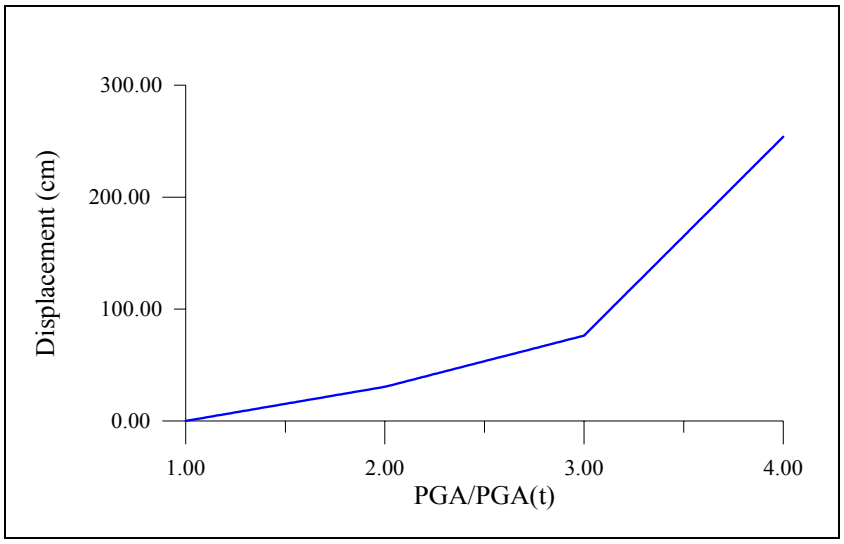

Figure 5.19: Lateral Spreading Displacement Relationship after [Youd and Perkins, 1978].

Susceptibility Category	*PGA* (t)
Very High	0.09 g
High	0.12 g
Moderate	0.15 g
Low	0.21 g
Very Low	0.26 g
None	N/A

Table 5.13: Threshold Ground Acceleration (*PGA*(t)) corresponding to zero Probability of Liquefaction.

Substituting M = 6.4 in equation 5.14, correction factor is: $K_{\Delta} = 0.534$ .Maximum considered Peak Ground Acceleration is: $PGA_{\max} = 3(0.1646)g = 0.4938g$ Then for Moderate category of Liquefaction susceptibility, ratio for Peak Ground Acceleration at the site and Threshold for Peak Ground Acceleration for the susceptibility category is:

$$\frac{PGA_{\max}}{PGA(t)} = \frac{0.4938}{0.15} = 3.292$$

For Low category of Liquefaction Susceptibility, ratio for Peak Ground Acceleration at the site and Threshold for Peak Ground Acceleration for the susceptibility category is:

$$\frac{PGA_{\max}}{PGA(t)} = \frac{0.4938}{0.21} = 2.351$$

According to the curve in Figure 5.19, the expected Permanent Ground Displacement for each category is:

Moderate Susceptibility:

$$E[PDG_{SC}] = K_{\Delta} \cdot E[PDG|(PGA/PL_{SC}) = a] = 0.689 \cdot 128.12\ cm = 88.264\ cm$$

Low Susceptibility:

$$E[PDG_{SC}] = K_{\Delta} \cdot E[PDG|(PGA/PL_{SC}) = a] = 0.689 \cdot 46.523\,cm = 32.05\,cm$$

Expected lateral spreading PGD'S are shown in Map 5.14, with the respective Liquefaction Probabilities for the soil deposits considered in this research.

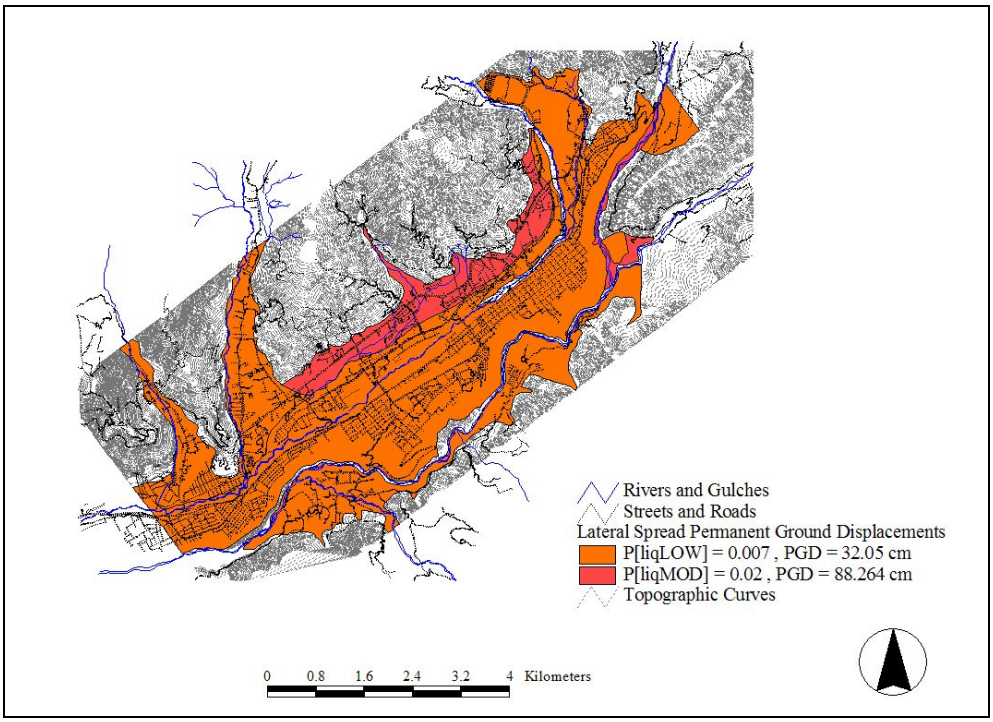

Map 5.14: Lateral Spread Permanent Ground Displacements, for *I* = IX Scenario Event.

Ground settlements associated with liquefaction are assumed to have a relationship with the susceptibility category of an area, in accordance with relations presented in [Tokimatsu and Seed, 1987] which indicate strong correlations between volumetric strain and soil relative density. Additionally, experiences have verified that deposits with higher susceptibility tend to have increased thickness of potential liquefiable soils. Estimation for expected ground settlements is the product of the probability of liquefaction for a determined susceptibility class (eq. 5.10) and the characteristic settlement amplitude to this susceptibility class (Table 5.14).

Equation for Expected Ground Settlement is:

$$E[GrS] = P[Liquefaction_{SC}] \cdot ChS_{SC} \qquad \text{eq. 5.15}$$

Where,

$P[Liquefaction_{SC}]$ is the liquefaction probability for a given susceptibility class, and

ChS_{SC} is the Characteristic Settlement for the Susceptibility Category of soil deposit.

Relative Susceptibility	Characteristic Settlement (m)
Very High	0.30
High	0.15
Moderate	0.06
Low	0.03
Very Low	0
None	0

Table 5.14: Ground Settlement Amplitudes for Liquefaction Susceptibility Categories [HAZUS-99-SR2, 2002].

For the case pertaining this research, expected ground settlement for the two susceptibilities in soil deposits considered are:

Moderate Susceptibility Soils:

$$E[GrS] = 0.02 \cdot 0.06\ m = 0.0012\ m$$

Low Susceptibility Soils

$$E[GrS] = 0.007 \cdot 0.03\ m = 0.00021\ m$$

For soil deposits liquefaction susceptibilities, a summary of results for potential liquefaction hazards, considered for the worst event in the scenarios: I = IX, M = 6.8, at 15 km distance from the source, with an annual exceedance probability of 0.0012, is shown in Table 5.15.

Liquefaction Susceptibility	Liquefaction Probability	Permanent Ground Displacements (m)	
		Lateral Spreading	Ground Settlement
Moderate	0.02	0.88264	0.0012
Low	0.007	0.3205	0.00021

Table 5.15: Summary results for Potential Liquefaction Hazards (I = IX scenario event).

Expected Permanent Ground Displacements (PGD) for Liquefaction Susceptibility Categories in soil deposits must be understood in the scope of which deformations and displacements probably may occur. Lateral Spreading is susceptible to occur in gentle slopes or near water bodies, as in Mérida's Tableau bodies of water are not present, gentle slopes must be identified and located as susceptible sites for this kind of liquefaction phenomenon, in this case, mostly the northern boundary of Colluvional soil deposits. Ground Settlements, as a ground-level liquefaction phenomenon, may occur at almost flat terrain. In the research case, these kinds of sites are located in the central stripe of the tableau, between Albarregas and Chama Rivers.

5.4.4.2 Landslide Susceptibility Assessment

Earthquake-induced landslides are the product of various confluent factors, such as geologic and hydrologic conditions, topography, climate, weathering, and land use. Several earthquake-induced landslide types exist based in material type (soil or rock), movement characteristics (disrupted or coherent), velocity, depth and water content. General classification divides earthquake-induced landslides into three main groups: Disrupted Slides and Falls, Coherent Slides and Lateral Spreads and Flows. For the methodology used in this research, the last group is included in the potential liquefaction assessment rather than in the landslide potential. Disrupted Slides and Falls and Coherent Slides types and characteristics are shown in Table 5.16.

Characteristics appearing in this table are as follows:

- Internal Disruption describes the type of geometrical arrange in material failure, "slight" stands for landslide consisting of one or a few coherent blocks; "moderate" for several coherent blocks; "high" for numerous small blocks and individual soil grains and rock fragments; and "very high" for nearly complete disgregation into individual soil grains or small rock fragments.
- Water Content: describes the groundwater condition with the following classes; D, dry; U, moist but unsaturated; PS, partially saturated; and, S, saturated.
- Velocity: describes the sliding movement velocity of the failure in meters, with the following relationship;

0.6 m/yr	1.5 m/yr	1.5 m/month	1.5 m/day	0.3 m/min	3 m/s	.
extremely slow	very slow	slow	moderate	rapid	very rapid	extremely rapid

- Depth: describes the thickness of the failure; "shallow" stands for failure thickness lower than 3 m; and "deep" for failure thickness greater than 3 m.

Frequencies of occurrence for the different types of landsliding are shown in Table 5.17, these are the results of 40 historical earthquakes study, it may be noted that rock falls, disrupted soil slides and rock slides are the most abundant, and the least abundant are those with subaqueous landslides, slow earth flows, rock block slides and rock avalanches.

The HAZUS® methodology for assessing landslide susceptibility considers slope failure occurrence when the static forces added to the inertia forces within the slide mass, generate a drop in the safety factor below 1.0. This drop in safety factor is caused by a certain value of Peak Ground acceleration within the slide mass, denoted as critical acceleration or yield acceleration a_c.

	Name	Type of Movement	Internal Disruption	Water Content				Velocity	Depth
				D	U	PS	S		
Disrupted Slides and Falls	Rock Falls	Bounding, rolling, free fall	High or Very High	x	x	x	x	Extremely Rapid	Shallow
	Rock Slides	Translational sliding on basal shear surface	High	x	x	x	x	Rapid to extremely rapid	Shallow
	Rock Avalanches	Complex, involving sliding and/or flow, as stream of rock fragments	Very High	x	x	x	x	Extremely Rapid	Deep
	Soil Falls	Bounding, rolling, free fall	High or Very High	x	x	x	x	Extremely Rapid	Shallow
	Disrupted Soil	Translational sliding on basal shear surface or zone of weakened, sensitive clay	High	x	x	x	x	Moderate to rapid	Shallow
	Soil Avalanches	Translational sliding with subsidiary flow	Very High	x	x	x	x	Very rapid to extremely rapid	Shallow
Coherent Slides	Rock Slumps	Sliding on basal shear surface with component of headward rotation	Slight or Moderate	?	x	x	x	Slow to rapid	Deep
	Rock Block Slides	Translational sliding on basal shear surface	Slight or Moderate	?	x	x	x	Slow to rapid	Deep
	Soil Slumps	Sliding on basal shear surface with component of headward rotation	Slight or Moderate	?	x	x	x	Slow to rapid	Deep
	Soil Block Slides	Translational sliding on basal shear surface	Slight or Moderate	?	?	x	x	Slow to rapid	Deep
	Slow Earth Flows	Translational sliding on basal shear surface with minor internal flow	Slight			x	x	Very slow to rapid with very rapid surges	Generally Shallow, occasionally Deep

Table 5.16: Types and Characteristics of Earthquake-Induced Landslides, after [Kramer, 1996].

Values for this parameter are determined based in the Newmark sliding block analysis, which provides a stability index (Safety Factor) expressed as the ratio between the available resisting force and the pseudo static driving force. Inertial forces in the block due to horizontal vibration of the inclined plane are exerted with acceleration $a_h(t) = k_h(t)g$, at a particular moment the block will induce a horizontal force $k_h W$ (see Figure 5.20), expression for the ratio, resolving the forces acting perpendicular to the plane is:

$$FS_d(t) = \frac{\text{available resisting force}}{\text{pseudostatic driving force}} = \frac{R_d(t)}{D_d(t)} = \frac{\left[\cos\beta - k_h(t)\sin\beta\right]\tan\phi}{\sin\beta + k_h(t)\cos\beta} \qquad \text{eq. 5.16}$$

where ϕ is the angle of friction between the block and the plane.

Abundance	Description
Very Abundant (>100,000 in the 40 earthquakes)	Rock falls, disrupted soil slides, rock slides
Abundant (10,000 to100,000 in the 40 earthquakes)	Soil lateral spreads, soil slumps, soil block slides, soil avalanches
Moderately Common (1,000 to10,000 in the 40 earthquakes)	Soil falls, rapid soil flows, rock slumps
Uncommon	Subaqueous landslides, slow earth flows, rock block slides, rock avalanches

Table 5.17: Relative Abundance of Earthquake-Induced Landslides from study of 40 Historical Earthquakes ranging from M_s = 5.2 to M_w = 9.5 [Kramer, 1996].

In equation 5.16, as k_h increases the factor of safety decreases, at some positive value for this parameter Safety Factor (SF) becomes 1.0 and it is named yield coefficient k_y, corresponding to the critical acceleration $a_c = k_y g$. This yield acceleration is the minimum pseudo static acceleration required to produce the instability of the block, and has the expression:

$$k_y = \tan(\phi - \beta) \qquad \text{eq. 5.17}$$

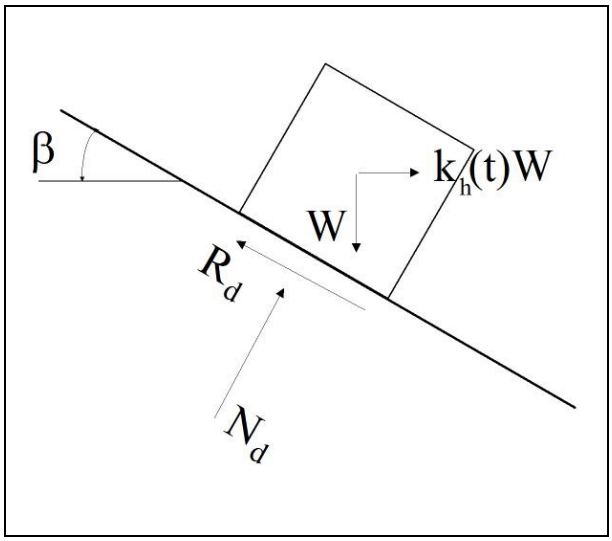

Figure 5.20: Forces acting on a block resting on an inclined plane under dynamic conditions.

Instability involves down-slope movement of the block; displacements are produced at time periods when the exerted acceleration exceeds the critical acceleration, $a_h(t) > a_c$. Displacements accumulate depending on the ratio of a_c to $a_h(t)$; generally, at smaller ratio (below 1.0) the greater is the number and duration of times for down-slope movements.

The relationship used for landslide critical acceleration is that of [Wilson and Keefer, 1985], shown in Figure 5.21, characterized by the geologic group for the soils in the interest zone, groundwater condition in soils, slope angle of terrain and critical acceleration.

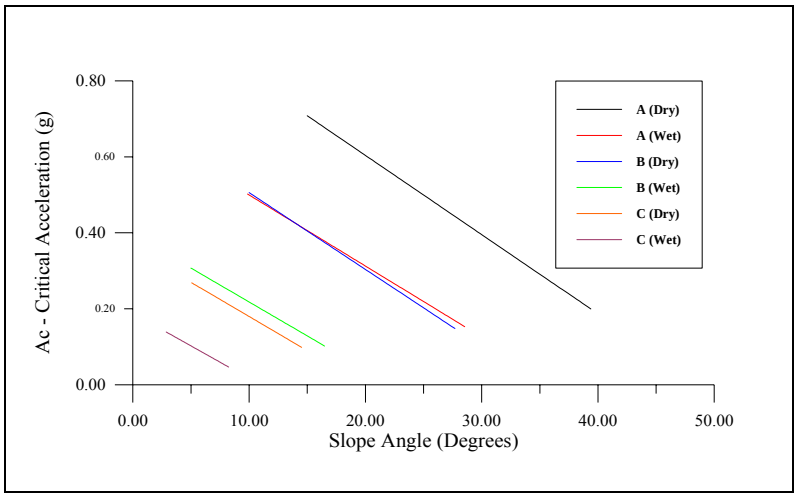

Figure 5.21: Critical Acceleration as Function of Geologic Group and Slope Angle [Wilson and Keefer, 1985]

Geologic Group		Slope Angle (Degrees)					
		0-10	10-15	15-20	20-30	30-40	>40
(a) DRY (Groundwater below level of sliding)							
A	Strongly Cemented Rocks (crystalline rocks and well cemented sandstone, $c' = 300\ psf, \phi = 35°$)	None	None	I	II	IV	VI
B	Weakly Cemented Rocks and Soils (sandy soils and poorly cemented sandstone, $c' = 0\ psf, \phi = 35°$)	None	III	IV	V	VI	VII
C	Argillaceous Rocks (shales, clayey soil, existing landslides, poorly compacted fills, $c' = 0\ psf, \phi = 20°$)	V	VI	VII	IX	IX	IX
(b) WET (Groundwater level at ground surface)							
A	Strongly Cemented Rocks (crystalline rocks and well cemented sandstone, $c' = 300\ psf, \phi = 35°$)	None	III	VI	VII	VIII	VIII
B	Weakly Cemented Rocks and Soils (sandy soils and poorly cemented sandstone, $c' = 0\ psf, \phi = 35°$)	V	VIII	IX	IX	IX	X
C	Argillaceous Rocks (shales, clayey soil, existing landslides, poorly compacted fills, $c' = 0\ psf, \phi = 20°$)	VII	IX	X	X	X	X

Table 5.18: Landslide Susceptibility for Geologic Groups [HAZUS-99-SR2, 2002].

Susceptibility Category	None	I	II	III	IV	V	VI	VII	VIII	IX	X
Critical Acceleration (g)	None	0.60	0.50	0.40	0.35	0.30	0.25	0.20	0.15	0.10	0.05

Table 5.19: Critical Acceleration for Susceptibility Categories [HAZUS-99-SR2, 2002].

Landslide Susceptibility assessment is performed by means of assigning a susceptibility category based in geologic group, groundwater conditions and slope angle from Table 5.18, as the susceptibility group is assigned, Critical Acceleration is then assessed from Table 5.19. As landslide susceptibility is assessed in the basis of a conservative approach [Wilson and Keefer, 1985], this aspect is considered by the use of a Map Area Percentage applied to susceptible sites (Table 5.20), based on [Wieczorec et. al., 1985]. Landsliding does or does not occur within susceptible deposits depending on whether the induced peak ground acceleration a_{is} exceeds or not the critical acceleration a_c, in a certain percentage of the total surface of the site assessed.

Susceptibility Category	None	I	II	III	IV	V	VI	VII	VIII	IX	X
Map Area	0.00	0.01	0.02	0.03	0.05	0.08	0.10	0.15	0.20	0.25	0.30

Table 5.20: Percentage of Map Area having a Landslide-Susceptible deposit [Wieczorec et. al., 1985].

Slope classification performed over Mérida's Tableau is shown in Map 5.15, slope intervals correspond to those of Table 5.18; the red line in the map indicates the border of the tableland towards the Chama River Canyon. Soil group for these steep slopes is not unique, due to the soil composition in three layers (Table 5.9); the surface and intermediate layers (weakly cemented rocks and soils) should be the most susceptible to landslide, while the deeper zone (strongly cemented rocks) should represent the least susceptible. In the face of slopes, it is possible that the three layers appear if the canyon is deep enough. For the interest of this research, a conservative approach is performed considering that the slopes are entirely composed by the soil group of the surface and middle layers, in this case belonging to geologic group B. Groundwater condition is WET for these sites, as water table level average is around 3 to 4 m, and may be considered at ground surface.

In Map 5.16, landslide susceptibility in Mérida's sites is shown. The most susceptible sites are located at the southern flank of the tableau in the Chama River border; with categories ranging from VIII to X. Critical accelerations for these categories range between values 0.15 and 0.05 g (Table 5.19). Account must be taken about the Map Area percentages corresponding to each of the susceptibility categories, then, for example, sites with susceptibility category X have a 30% of the Map Area susceptible to landslide. Based in the latter, it may be stated that special attention must be paid to sites at the southern stripe of the tableau, which also has important parts of the city's facilities and buildings.

It is important to observe that amplifications were assessed in the tableau itself; thus, information pertaining amplification factors and periods of amplification outside the limits of the tableland are not available as results from this research.

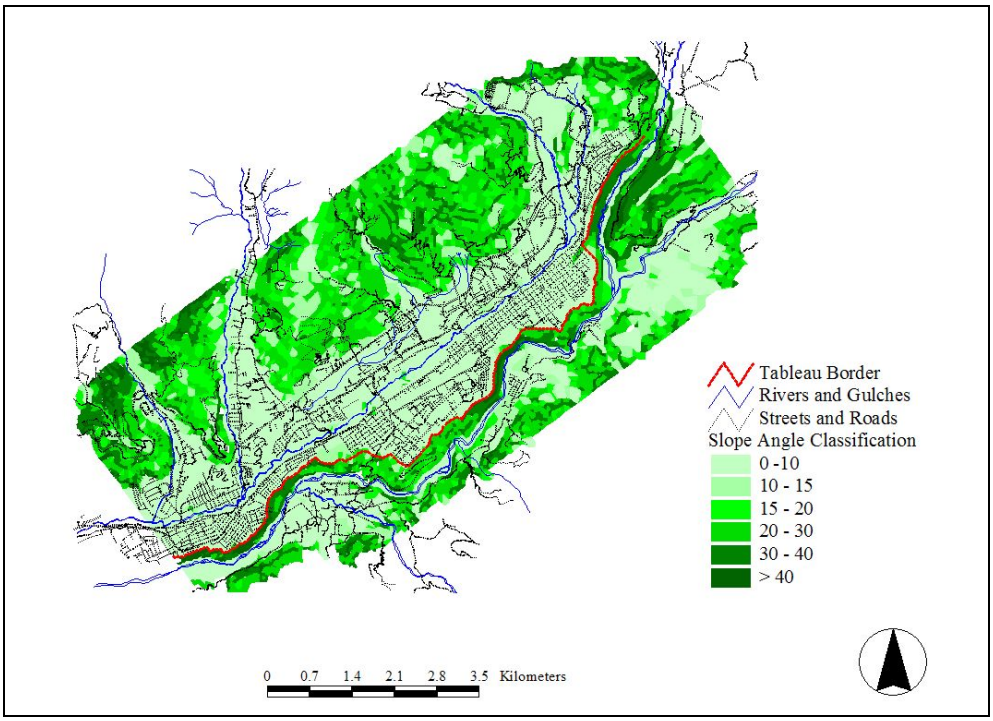

Map 5.15: Slope Classification for analysis.

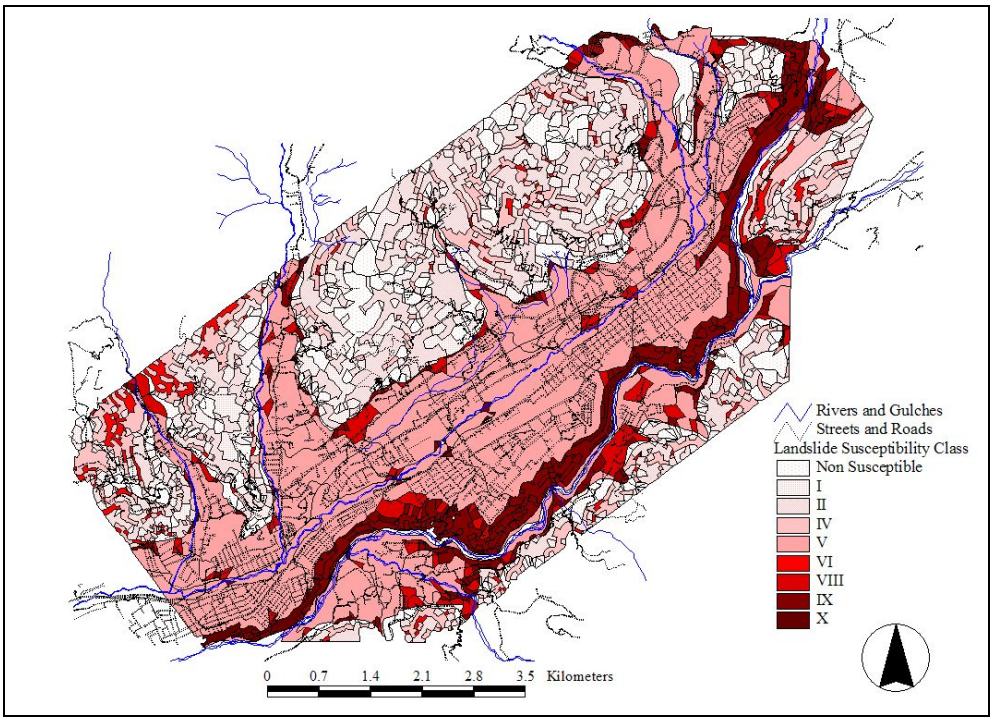

Map 5.16: Landslide Susceptibility Map for Mérida's tableau.

However, composition for the mountains around Mérida's Tableau is fractured rock and massive rock, as outcropping bedrock appears where the soils end at the northerly and southerly foothills. It is considered then, that earthquake-induced accelerations in these sites are those of the scenario events, estimated by the attenuation laws. The HAZUS® methodology recommends that induced peak ground acceleration in sites with these

characteristics a_{is} must be assumed the same as those predicted by the ground acceleration attenuation law used.

Induced peak ground accelerations employed for landslide assessment in this research are those of the scenario events obtained through the attenuation law used in hazard evaluation.

Permanent Ground Displacements (PGD in centimeters) estimation for landslide susceptible deposits is performed in the basis of the following expression:

$$E[PGD] = E[d/a_{is}] \cdot a_{is} \cdot n \qquad \text{eq. 5.18}$$

Where,

$E[d/a_{is}]$ is the expected displacement factor

a_{is} is the induced acceleration (in decimal fraction of g's)

n is the number of cycles (eq. 5.19)

The relationship between the number of cycles and earthquake moment magnitude M [Seed and Idriss, 1982] is expressed as:

$$n = 0.3419M^3 - 5.5214M^2 + 33.6154M - 70.7692 \qquad \text{eq. 5.19}$$

Relationships for expected displacement factor (Figure 5.22) are derived from the results of [Maksidi and Seed, 1978], where the displacement factor d/a_{is} is calculated as a function of the ratio a_c/a_{is}. The range in estimated displacement factor is shown by the upper and lower bounds of the relationship, with a uniform probability distribution of displacement factors between both bounds.

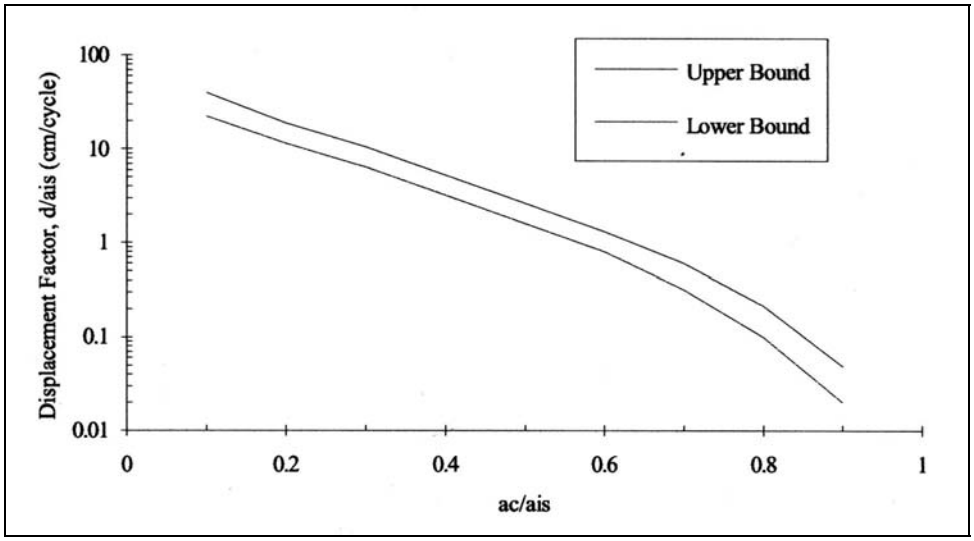

Figure 5.22: Relationship between Displacement Factor and Ratio of Critical Acceleration-Induced Acceleration [HAZUS-99-SR2, 2002].

For the case pertaining this research, Ratio between Critical Acceleration for each landslide susceptibility category and Induced Peak Ground Acceleration is estimated for every scenario event considered; results are shown in Table 5.21. The values for ratio a_c/a_{is} are lower than 1.0 for scenario event I = IX, at sites with susceptibility categories from VIII to X; for scenario events I = VII and I = VIII, at sites with susceptibility categories IX and X; and for scenario event I = VI, at sites with susceptibility category X (bold style values in Table 5.21). Landslide may occur within these susceptibility categories.

Susceptibility Category	I	II	III	IV	V	VI	VII	VIII	IX	X
Critical Acceleration (g)	**0.6**	**0.5**	**0.4**	**0.35**	**0.3**	**0.25**	**0.2**	**0.15**	**0.1**	**0.05**
Ratio for *I*=VI	6.7416	5.618	4.4944	3.9326	3.3708	2.809	2.2472	1.6854	1.1236	**0.5618**
Ratio for *I*=VII	5.231	4.3592	3.4874	3.0514	2.6155	2.1796	1.7437	1.3078	**0.8718**	**0.4359**
Ratio for *I*=VIII	4.2194	3.5162	2.8129	2.4613	2.1097	1.7581	1.4065	1.0549	**0.7032**	**0.3516**
Ratio for *I*=IX	3.6452	3.0377	2.4301	2.1264	1.8226	1.5188	1.2151	**0.9113**	**0.6075**	**0.3038**

Table 5.21: Ratio between Critical Acceleration and Induced Peak Ground Acceleration for each Landslide Susceptibility Category.

Part of the results visualization is shown in Map 5.17, where a_c / a_{is} ratio for scenario event *I* = IX is plotted. Values are divided into two classes: one for ratio below or equal to 1.0 and the other for ratio greater than 1.0. This allows identifying easily in the map the sites where landslide may take place due to the occurrence of an event of those characteristics.

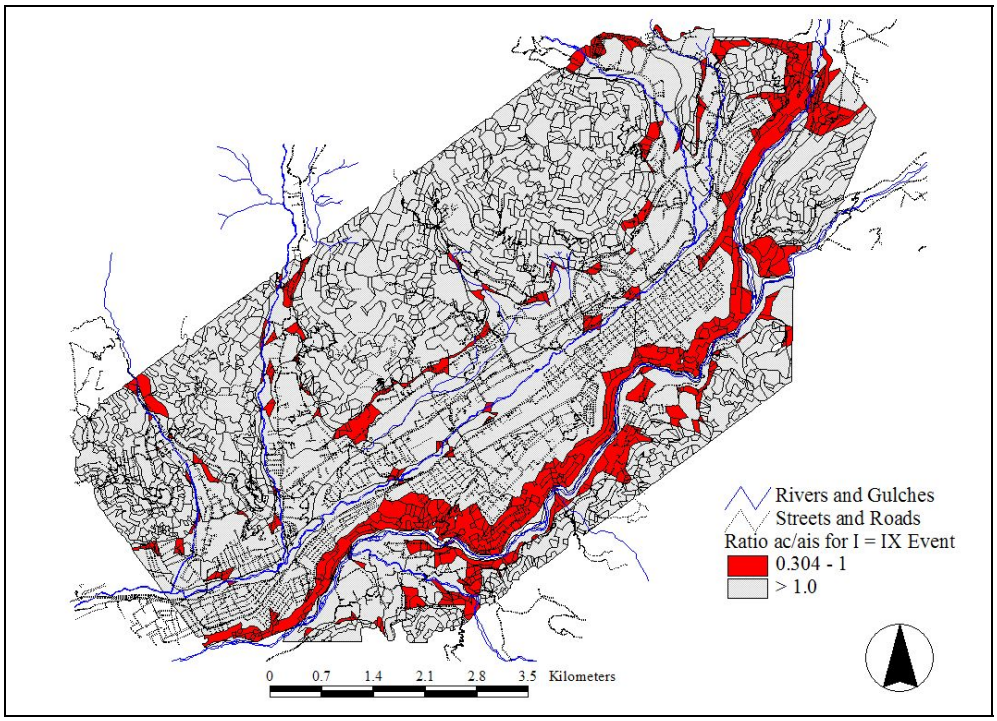

Map 5.17: Critical Acceleration/Induced Acceleration Ratio for Scenario Event *I* = IX.

Permanent Ground Displacements (in centimeters) are estimated for all scenario events using equation 5.18, and are shown in Table 5.22. PGD's results visualization for scenario event *I* = IX are shown in Map 5.18, displacements are distributed mostly over the Chama and Mucujún rivers canyons, as previously identified in Map 5.17.

Susceptibility Category	I	II	III	IV	V	VI	VII	VIII	IX	X
PGD for *I*=VI	None	None	None	None	None	None	None	None	None	0.3219
PGD for *I*=VII	None	None	None	None	None	None	None	None	0.0237	1.7787
PGD for *I*=VIII	None	None	None	None	None	None	None	None	0.4459	6.689
PGD for *I*=IX	None	None	None	None	None	None	None	0.0494	1.6477	14.8292

Table 5.22: Permanent Ground Displacements (cm) for scenario events considered.

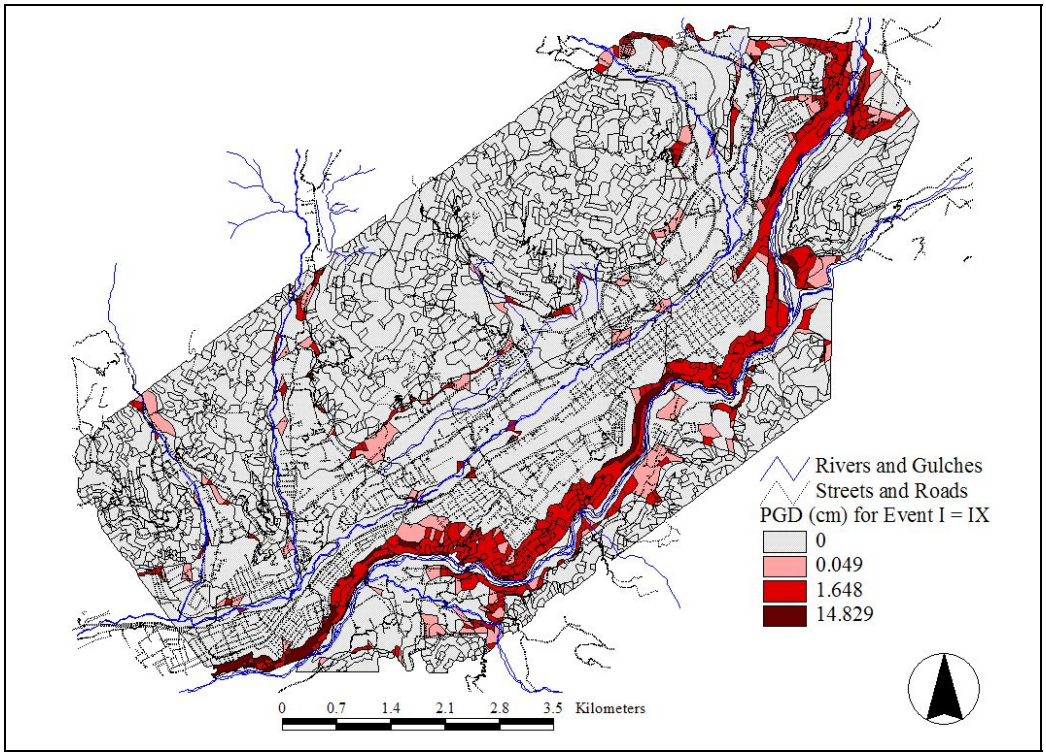

Map 5.18: Landslide Permanent Ground Displacements for *I* = IX scenario event.

The following maps (Map 5.19, Map 5.20 and Map 5.21) show landslide Permanent Ground Displacements for the other three scenario events considered in this research. Landslides represent a considerable hazard for scenario events *I* = VIII and *I* = IX, localized over the southerly border of the tableau in the Chama River flank, if landslide occurs, this part of the city may disappear or be severely damaged and soil falls may dam the river and/or block the roads to the southeastern sectors of the city.

For scenario events *I* = VII and *I* = VI (Map 5.20 and Map 5.21), PGD's values are lower than in other events. This indicates that although landslides occur, the effects may be localized, not compromising great areas of the city, however, facilities and lifelines locations must be assessed in order to estimate the particular effects that small landslides may produce over these.

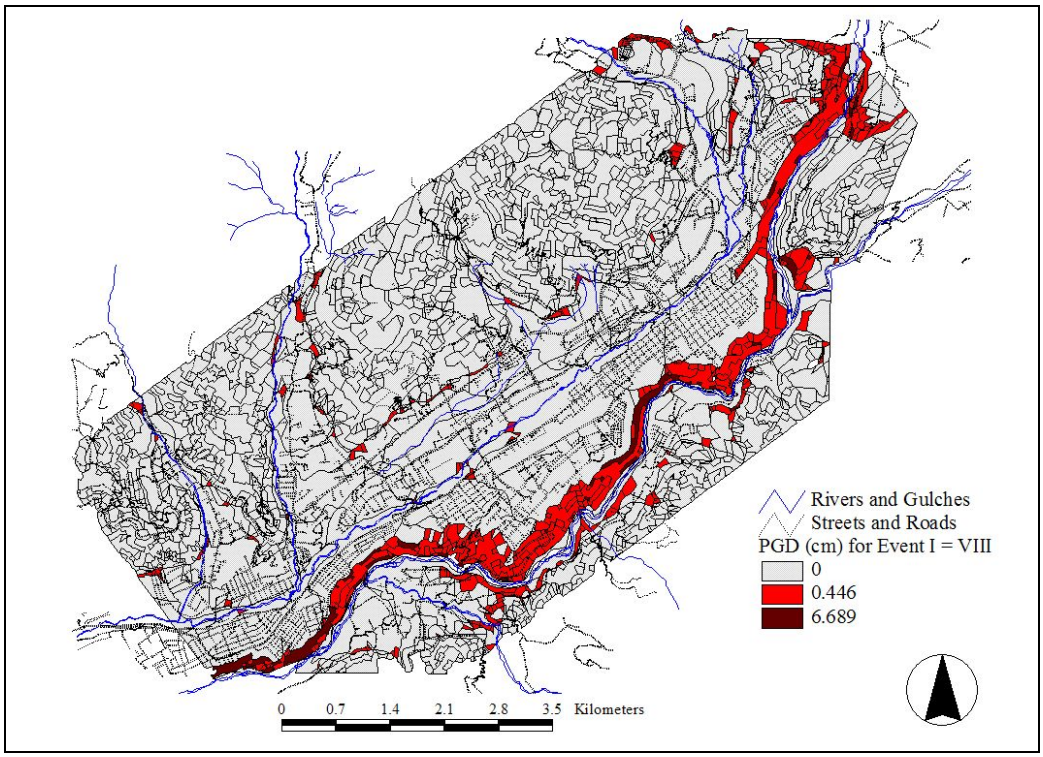

Map 5.19: Landslide Permanent Ground Displacements (cm) for *I* = VIII scenario event.

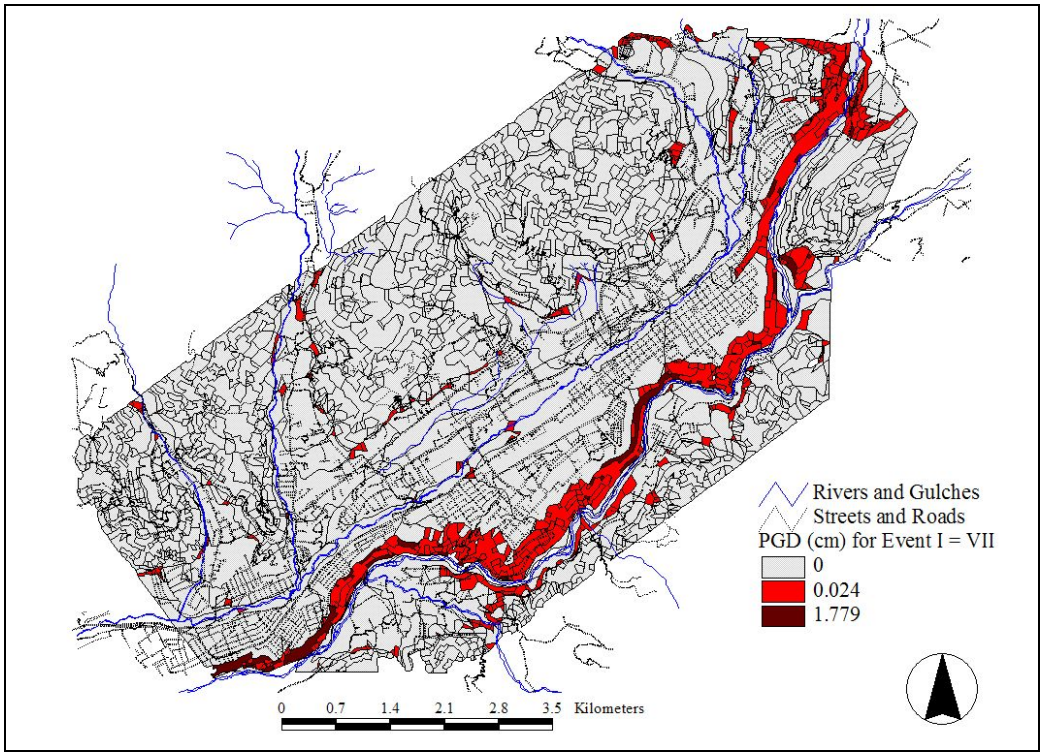

Map 5.20: Landslide Permanent Ground Displacements (cm) for *I* = VII scenario event.

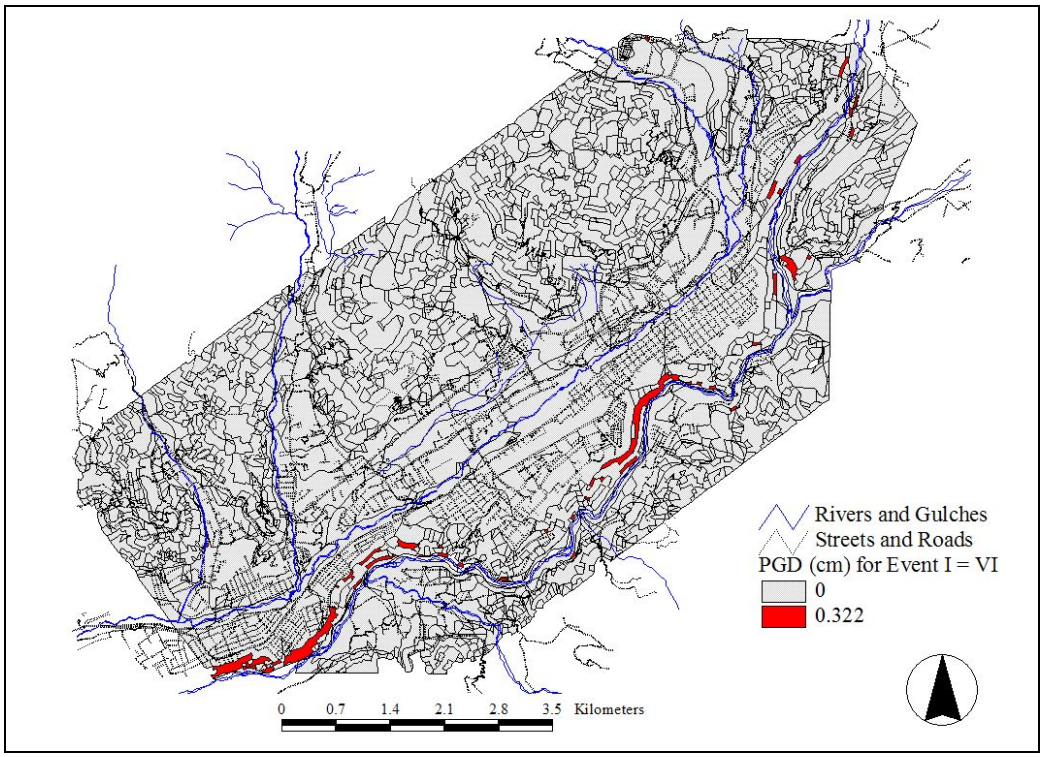

Map 5.21: Landslide Permanent Ground Displacements (cm) for *I* = VI scenario event.

Permanent Ground Displacements produced by phenomena such as liquefaction and landslide may generate considerable damage to built environment and consequently distribute losses of different nature (human, economic and social), further in this research, issues concerning these aspects are treated as part of the seismic risk evaluation for Mérida city.

5.5 Summary

The population in Venezuela is mostly concentrated in cities over a tectonic stripe with evidences of recent activity and where historical damaging events have occurred. This tectonic stripe is identified by the presence of mountain chains in all its longitude crossing the country from East to West in front of the Caribbean Sea from the central coast to the eastern coast and from northeast to southwest in the western portion of Venezuela. The most important seismogenic source in western Venezuela is the Boconó Fault Zone, which includes the city of Mérida in its path through the Andean Mountain range. Probabilistic seismic hazard analysis results in four scenario events corresponding through the attenuation law considered, to events with Intensities from *I* = VI to *I* = IX (see Table 5.8).

The site response analysis performed shows a difference in response spectra for the two soils at either side of the Albarregas River, where southerly sites may produce amplification factors up to a 14% greater than in the northerly sites. Average value for the amplification factors are around 2.5 times the input at outcropping rock. The periods for maximum amplification in the response spectra for both soil types are between 0.20 s and 0.25 s. A local intensity map (Map 5.8), based in the conversion of the amplification into variations of the intensity degree, shows that soils at southerly Albarregas River (with first layer thicknesses between 4 m to 10 m and soils with first layer thickness of 20 m) are expected to increase the intensity degree up to a middle value of intensity.

The potential induced effects of liquefaction and landsliding are assessed through the HAZUS®99 [HAZUS-99-SR2, 2002] methodology. The results (for the last scenario event)

show a low (in around an 88% of the tableau's surface) to moderate (in around a 12% of the tableau's surface) liquefaction susceptibility for Mérida's soils (Table 5.15, Map 5.14). The landsliding susceptibility is concentrated over the high-slope canyons of the Chama and Mucujún rivers in the tableau's southeastern border (Map 5.18).